Industrial Chemistry & Materials

ROYAL SOCIETY OF CHEMISTRY

REVIEW

View Article Online
View Journal | View Issue

Cite this: *Ind. Chem. Mater.*, 2025, **3**, 151

In situ polymerization of fluorinated electrolytes for high-voltage and long-cycling solid-state lithium metal batteries

Yunpei Lu,[a] Xinyi Zhang,[a] Yong Wu,[ab] Hao Cheng[ab] and Yingying Lu *[ab]

Currently, the practical application of liquid lithium-ion batteries faces challenges in meeting the requirements of high energy density and safety. To address concerns such as electrolyte leakage and flammability, solid polymer electrolytes (SPEs) have emerged as promising alternatives to liquid electrolytes. SPEs, particularly those synthesized *via in situ* polymerization processes, offer advantages in establishing robust interface contacts and compatibility with existing industrial production lines. However, the electrochemical stability of SPEs remains a hurdle for high-voltage lithium metal batteries (LMBs). To enhance interface uniformity, electrochemical stability, and thermal stability, researchers commonly employ fluorination strategies, thus expanding the potential of SPEs in high-voltage, long-cycling LMBs. Fluorine plays a crucial role in achieving these objectives due to its high electronegativity, polarization, outstanding dielectric properties, strong bond strength, stability, and hydrophobic nature. In this study, we delve into how fluorinated electrolytes improve interface stability between SPEs and electrodes by examining their underlying mechanisms. Besides, we provide an overview of current fluorination strategies and their impact on battery performance. Furthermore, we discuss challenges and issues associated with current *in situ* polymerized fluorinated SPE routes and propose practical strategies for consideration.

Keywords: Lithium metal batteries; *In situ* polymerization; Fluorinated polymer electrolytes; High-voltage; Long cycling; Stable interface.

Received 4th July 2024,
Accepted 12th September 2024

DOI: 10.1039/d4im00082j

rsc.li/icm

[a] *State Key Laboratory of Chemical Engineering, Institute of Pharmaceutical Engineering, College of Chemical and Biological Engineering, Zhejiang University, Hangzhou 310027, China. E-mail: yingyinglu@zju.edu.cn*
[b] *ZJU-Hangzhou Global Scientific and Technological Innovation Centre, Zhejiang University, Hangzhou 311215, China*

1. Introduction

Li-metal has been considered the "holy grail" anode material for next-generation high-energy rechargeable batteries due to

Yunpei Lu

Yunpei Lu is currently a postgraduate student in the College of Chemical and Biological Engineering, Zhejiang University under the supervision of Professor Yingying Lu. She received her B.S. degree in College of Chemical Engineering and Technology from Sun Yat-sen University in 2023. Her research is focused on high-energy-density long-cycling lithium metal batteries and solid polymer electrolytes.

Yingying Lu

Dr. Yingying Lu is the Qiushi Distinguished professor in the College of Chemical and Biological Engineering at Zhejiang University. Her research interests include nanomaterials, ionic liquids, and electrochemical energy storage and conversion. She received her B.S. degree in Chemical Engineering from Zhejiang University in 2010 and her Ph.D. from Cornell University in 2014. Afterward, she worked as a postdoctoral fellow in the Department of Materials Science and Engineering at Stanford University. Dr. Lu joined Zhejiang University as a tenure-track professor in 2015, and was promoted to Professor in 2022.

its high theoretical capacity (3860 mA h g^{-1}) and low electrochemical potential (−3.04 V *vs.* standard hydrogen electrode).[1] However, due to its low electrochemical potential, side reactions between the liquid electrolyte and Li-metal continue to occur. Furthermore, traditional organic electrolytes suffer from issues such as volatile leakage, flammability, and explosion, which fail to meet higher safety standards.[2,3] Replacing the liquid electrolyte with a solid electrolyte seems to be an effective way to address the safety problems of LMBs. Among the various types of solid electrolytes, SPEs show enormous potential due to their high flexibility and excellent processability. However, traditional SPEs are typically synthesized separately and then assembled into batteries. Compared to *ex situ* SPEs, *in situ* SPEs have better contact and stability at the electrolyte–electrode interface, simplify the manufacturing process, and offer significant advantages in the development and application of solid-state LMBs.

The first report of SPEs created through *in situ* polymerization for lithium batteries dates back to 1997.[4] By injecting a precursor solution containing low-viscosity monomers, lithium salts, and initiators evenly mixed into the battery, most pores in the electrodes and supported membrane are filled with the precursor solution. The supported membrane, placed between the cathode and anode, provides mechanical strength and prevents short circuits. Under external conditions (such as thermal initiation), the precursor within the battery polymerizes into an SPE, which tightly adheres to the electrode surface, significantly improving interfacial compatibility (Fig. 1). In addition, this method allows for the simultaneous synthesis of SPEs and battery assembly, making it compatible with "roll-to-roll" battery production lines and reducing costs. Moreover, *in situ* polymerization eliminates the complicated processes of polymer dissolution, membrane drying, and swelling associated with *ex situ* polymerization.[5]

However, there are still some obstacles in developing batteries assembled with *in situ* SPEs. One of the main obstacles is regulating the passivated electrode–SPE interphases. Side reactions happening between the electrodes and SPE might lead to the breakdown of mechanically fragile and chemically unstable interphases. On the side of the anode, Li-metal is highly reactive with SPEs, leading to two main issues: (1) rapid capacity fading caused by the irreversible cycling of lithium, and (2) uneven deposition of lithium, which causes dendrite growth and can puncture the electrolyte, resulting in safety issues.[2,3] On the side of the cathode, the catalytic activity of transition metal ions in cathode materials may further promote side reactions between the cathode and SPEs, leading to the formation of an unstable cathode–electrolyte interphase (CEI) and further continuous degradation. Moreover, the volume changes in cathode materials under high voltage can cause fractures at the CEI, reducing the contact area, and consequently decreasing the utilization of active materials, battery capacity, and cycle performance. For example, during the charge–discharge cycles of single-crystal NCM811, the accumulation of lattice rotation over time can exacerbate morphological and structural damage, resulting in a series of micro-cracks, irreversible phase transitions, and surface structure degradation, leading to severe electrochemical decay.[6] SPEs can be classified as all-solid-state polymer electrolytes (ASSPEs) and gel polymer electrolytes (GPEs), depending on whether liquid electrolyte content is added or not. ASSPEs are made up of pure lithium salts and conductive polymer matrixes, while GPEs contain 20–30 wt% liquid electrolytes, lithium salts and polymer matrixes.[7] Abundant polymer matrixes like poly(ethylene oxide) (PEO) and polycarbonate (PC) have been the most commonly used polymer matrixes. PEO has strong salt dissociation (dielectric constant = 8) and its ionic conductivity (IC) at room temperature (RT) is 10^{-6}–10^{-8} S cm^{-1}, which is lower than the level of practical

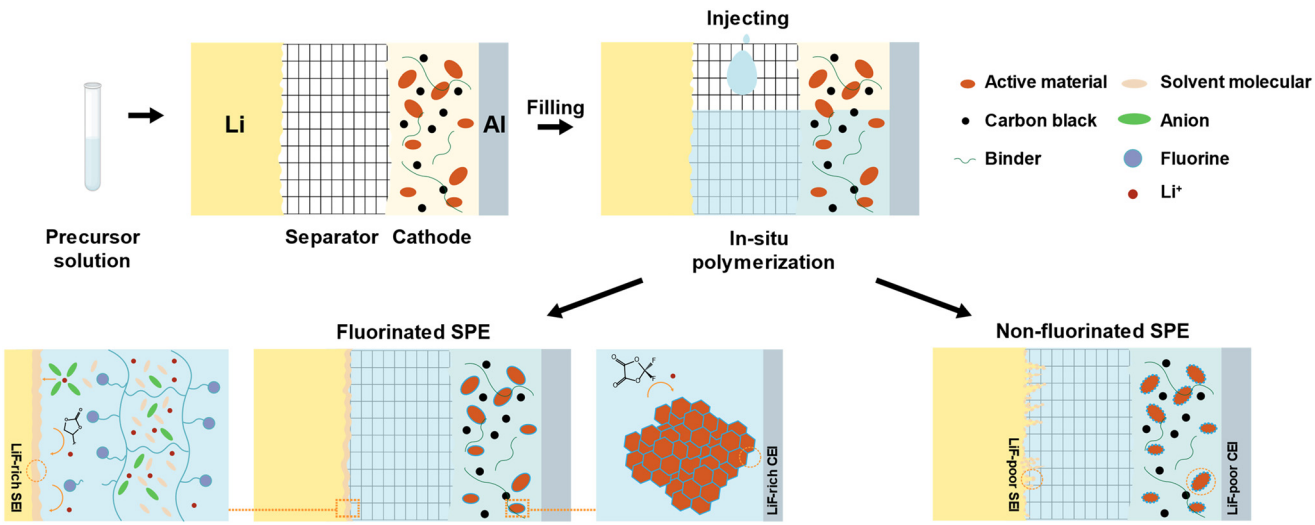

Fig. 1 Schematic of *in situ* polymerization of a fluorinated SPE *vs.* a non-fluorinated SPE.

application. The electrochemical stability window (ESW) of PEO is relatively low (ESW < 4.0 V), making it prone to degradation under high voltage conditions and only to be compatible with low voltage cathode materials (*e.g.* $LiFePO_4$, LFP).[8] PCs like poly(methyl methacrylate) (PMMA), poly(propylene carbonate) (PPC) and poly(vinyl carbonate) (PVC) with strong polar groups are able to dissolve lithium salts and reduce the tendency of ion agglomeration, which have a higher dielectric constant than PEO.[9] The ester groups have higher oxidation resistance compared to the ether groups.[10] However, drawbacks like poor interface compatibility with Li-metal, low ionic conduction and weak mechanical properties still limit their practical application.

The introduction of fluorine-containing materials can effectively address these issues. Firstly, the fluorinated solid electrolyte interphase (SEI) derived from fluorinated salts, solvents, and polymer chains can significantly suppress the formation of lithium dendrites and ensure the uniform deposition of Li^+ (Fig. 1). This enhancement contributes to batteries with ultra-long cycling lifespans. Secondly, a fluorinated CEI, originating from these fluorine-containing materials, prevents direct contact between the SPE and the cathode surface (Fig. 1). This inhibition of irreversible phase changes and the dissolution of transition metal elements in cathode materials mitigates the accelerated breakdown of electrolytes caused by high-valence nickel at elevated voltages.[11] Consequently, this reduces the capacity loss in batteries. Moreover, a robust fluorinated CEI endows the SPE with a higher ESW, allowing it to withstand oxidation at higher voltages, thus enhancing the energy density of batteries.[12] Fluorine-containing materials in the bulk phase further improve the thermal stability and ionic transport capability of the entire SPE. The carbon–fluorine (C–F) bond in the SPE backbone is among the strongest known, offering high thermal stability and non-flammability,[13] which significantly reduces safety risks such as fires or explosions. Additionally, the diverse coordination of Li^+ ions creates highly polar C–F$\cdots$$Li^+$ structures in the polymer backbone, forming new pathways for lithium ion transport and enhancing IC.[14] The fluorinated functional groups on the polymer also interact with anions from lithium salts, inhibiting their migration.[15,16] Furthermore, the electron density delocalization caused by fluorinated groups reduces the nucleophilicity of oxygen in the electrolyte, weakening its binding with Li^+. This increases the Li^+ transference number, further improving the performance and safety of the batteries.

In this review, we focus on the recent advances in the *in situ* polymerization of fluorinated SPEs. We explore the fundamental mechanisms behind the formation of fluorinated SEIs and CEIs and summarize the current advanced characterization techniques related to fluorinated SEIs/CEIs. We discuss the impacts on battery performances of different manufacturing processes (*ex situ vs. in situ*) of SPEs. Furthermore, we delve into how fluoromonomers and initiators affect the *in situ* polymerization process, which further improve battery performance in terms of electrochemical stability, interface stability, cycling lifespan, and fire-retardant efficiency. To provide a realistic outlook, we conclude by addressing the current limitations and challenges of fluorinated polymer electrolytes synthesized *via in situ* polymerization.

2. Characteristics of fluorinated electrolytes

An ideal highly electrochemically stable SPE should have no interfacial parasitic reactions with the electrode because all components of the SPE (lithium salts, polymers, and additives) should have their highest occupied molecular orbital (HOMO) energy levels below the cathode potential (μ_C), and their lowest unoccupied molecular orbital (LUMO) energy levels above the anode potential (μ_A). However, in practice, during the lithium deintercalation/intercalation process, the oxidation/reduction states can dynamically shift μ_C and μ_A to lower and higher energy levels respectively, compared to the HOMO/LUMO levels of the SPE (Fig. 2a).[17] Some components in the SPE (*e.g.*, LiDFOB and FEC) with narrow energy level gaps may undergo active decomposition, forming a protective SEI/CEI layer on the electrode surface. Therefore, to maintain a stable state during long-term cycling, it is crucial to form chemically passivated layers: a CEI on the cathode surface and an SEI on the Li-metal surface.

The composition of SPEs can include: a polymer matrix, lithium salts, solvents (present in GPEs, but not in ASSPEs), and additives. Based on their composition, fluorinated SPEs can generally be categorized into two types: (1) SPEs with a polymer matrix containing fluorine groups, and (2) SPEs with a non-fluorinated polymer matrix that incorporates fluorinated compounds in the form of lithium salts, additives, or solvents.

2.1. Mechanism of fluorinated electrolytes affecting formation of SEIs

Nowadays, it is generally accepted that the mainstream structures of the SEI are the double layer model[23,24] and the mosaic model,[25] both validated by cryogenic electron microscopy (cryo-EM).[26] According to these models, the SEI consists of two distinct regions. The outer region is primarily composed of organic species formed from the decomposition of organic solvents, including hemicarbonates and oligomers.[27] The inner region mainly consists of inorganic species such as LiF, Li_2CO_3, Li_2O, and Li_3N, which are both thermodynamically stable and non-degradable. These inorganic species exhibit varying electronic transfer abilities and ionic migration barriers, ranked as follows: LiF > Li_2CO_3 > Li_2O > Li_3N.[28,29] LiF also has a higher ESW (6.3 V *vs.* Li-metal) compared to other lithium binary compounds (3.1, 3.6, and 4.2 V *vs.* Li-metal for Li_2O, LiBr, and LiCl, respectively).[30] Consequently, LiF is a crucial component in

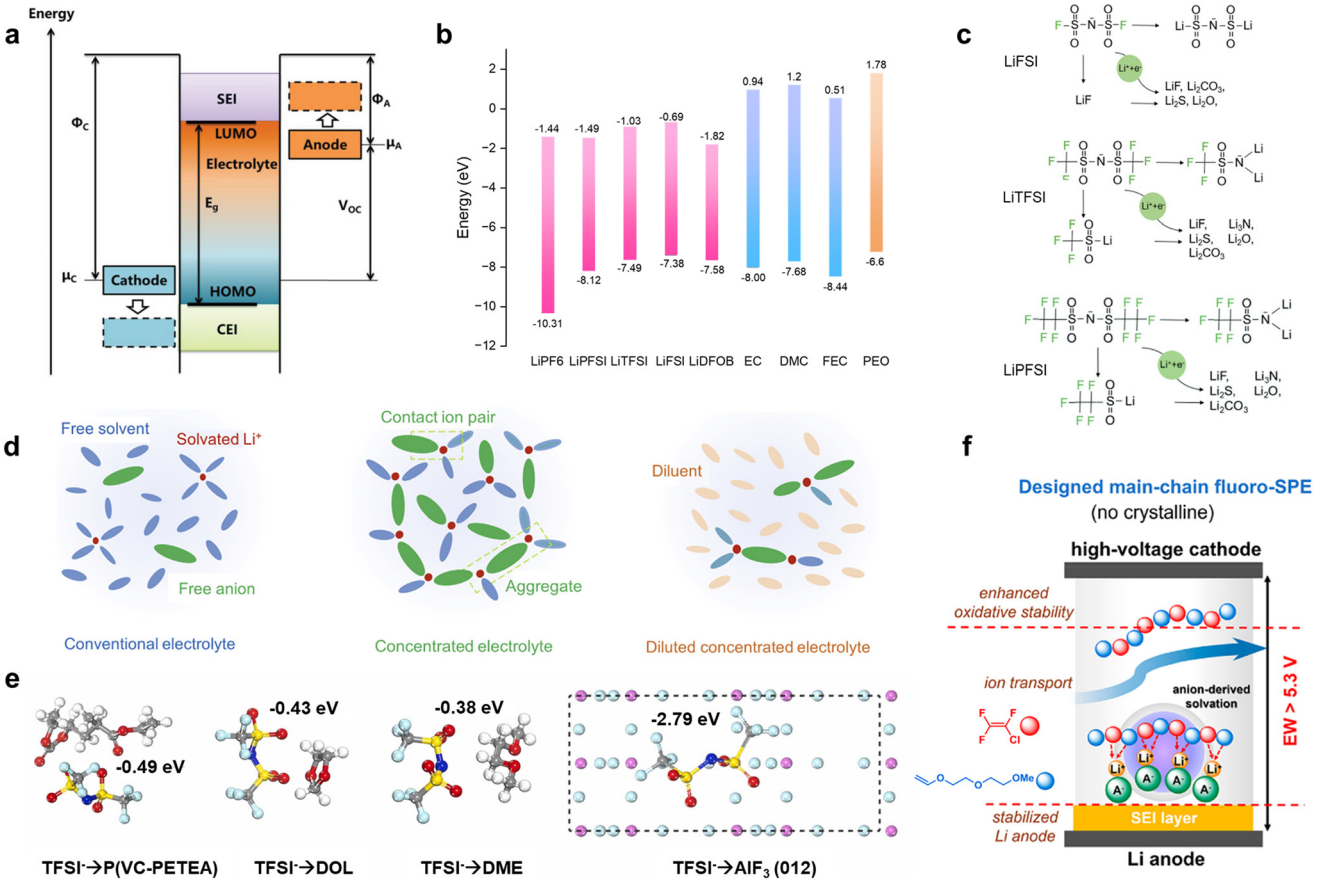

Fig. 2 Mechanism of anion-derived fluorinated SEIs. (a) Schematic diagram showing the working voltage *vs.* the energy levels of electrolyte at the open-circuit state. Reproduced with permission.[17] Copyright 2019, John Wiley and Sons; (b) HOMO and LUMO energies for commonly used lithium salts, solvents and SPEs. Reproduced with permission.[18] Copyright 2023, Springer Nature; (c) mechanism of LiFSI, LiTFSI and LiPFSI degradation to form SEIs. Reproduced with permission.[19] Copyright 2023, John Wiley and Sons; (d) illustrations of solution structures of three electrolytes: conventional electrolyte, concentrated electrolyte and diluted concentrated electrolyte. Reproduced with permission.[20] Copyright 2019, Springer Nature; (e) adsorption energy of $TFSI^-$ with electrolyte components of P(VC–PETEA), DOL, DME and AlF_3 (012) plane. Reproduced with permission.[21] Copyright 2023, Elsevier; (f) mechanism of main-chain fluorination enhancing the SEI *via* the intensified formation of anion-derived solvation structure. Reproduced with permission.[22] Copyright 2021, American Chemical Society.

producing a continuous and dense SEI because it effectively blocks electrons and supports the steady transport of Li^+ within the SEI. This section will discuss the formation mechanism of LiF in the SEI. It is known that the source of fluorine can be obtained from lithium salts, fluorinated additives, fluorinated solvents and fluorinated polymer segments. Since fluorinated polymer segments can also regulate the solvation of lithium ions like solvent molecules, we regard them as a macromolecular solvent in a broad sense. In summary, this section divides the formation mechanism of SEIs into two categories based on the source of fluorine: anion-derived fluorinated SEIs and solvent-derived fluorinated SEIs.

Anion-derived fluorinated SEIs. Lithium salts, such as lithium hexafluorophosphate ($LiPF_6$), bis-trifluoromethanesulfonimide (LiTFSI), lithium bis(fluorosulfonyl)imide (LiFSI), lithium tetrafluoroborate ($LiBF_4$), and lithium difluoro(oxalato)borate (LiDFOB), can provide fluorine for constructing salt-derived fluorinated SEIs. Density functional theory (DFT) calculations illustrate that lithium salts like $LiPF_6$, LiTFSI, LiFSI, and LiDFOB have lower LUMO energy levels than SPEs like ether-based PEO, suggesting the preferential decomposition of lithium salts over PEO. Additionally, all lithium salts exhibit lower HOMO energy levels than PEO, indicating that adding these lithium salts can improve the anti-oxidation ability of SPEs (Fig. 2b).[18] Li *et al.* discovered that LiTFSI and LiPFSI have a lower LUMO energy than LiFSI and thus can be easily decomposed. They studied the degradation mechanism of three lithium salts: LiFSI, LiTFSI, and lithium bis(penta-fluoroethanesulfonyl)imide (LiPFSI), (Fig. 2c).[19] They found that LiFSI tends to undergo four-electron reactions generating LiF and Li_2O species, while other reactions involving 8–16 electron transfers producing Li_3N and Li_2S species occur less frequently. Budi *et al.* also confirmed that no Li_3N species form from LiFSI in the SEI.[31] In contrast, LiTFSI and LiPFSI can generate Li_3N species in the SEI. It is concluded that the F-connecting bond is more significant than the molecular size and F element content. Additionally, the preferential cleavage of C–F bonds in LiPFSI is related to

their proximity to Li-metal; the closer to Li-metal, the easier the cleavage of the bonds. Consequently, the Li|Li symmetrical battery assembled with PEO containing LiPFSI is able to run steadily for over ~2700 h which is longer than that of LiFSI and LiTFSI, indicating that it has better lithium metal reversibility for the reason that LiPFSI creates a more robust and denser SEI.

To construct an inorganic species-rich SEI layer, highly concentrated electrolytes (HCEs) have been proposed for liquid electrolytes.[32] Compared with conventional electrolytes, there are barely any free solvents in the solvation sheath of lithium ions and abundant aggregates (AGGs) and contact ion pairs (CIPs) in HCEs (Fig. 2d),[20] which easily result in the formation of anion-derived fluorinated SEIs. However, HCEs suffer from high viscosity and high cost. Therefore, diluted conventional electrolytes (DCEs) have been proposed, which reduce viscosity and improve the wettability of electrolytes while maintaining the solvation structure of HCEs.[33] Similarly, this approach is also suitable for constructing solvation sheaths with rich AGGs and CIPs of lithium ions in SPEs. Various additives/solvents have been used to form CIPs or AGGs of lithium ions to dramatically improve lithium deposition behaviour.

Zhang *et al. in situ* synthesized an SPE, P(VC–PETEA), with the addition of AlF_3 additive.[21] DFT calculations show a strong attraction effect between $TFSI^-$ and the dominant AlF_3 (012) plane, with an adsorption energy (AE) as high as 2.79 eV, which is higher than that between $TFSI^-$ and P(VC–PETEA), 1,3-dioxolane (DOL) and 1,2-dimethoxyethane (DME) respectively, due to the electrostatic interaction between highly electronegative oxygen and nitrogen atoms and centric aluminium atoms on the surface of AlF_3 (Fig. 2e). This helps anchor $TFSI^-$ to form the anion-derived fluorinated SEI and promotes the migration of a significant number of free lithium ions. Thanks to the AlF_3 additive, highly lithiophilic Li–Al alloy, LiF-rich, and AlF_3 species are found in the SEI layer. The lithiophilic Li–Al alloy and AlF_3 species enable low nucleation and diffusion overpotential for Li deposition, while LiF effectively inhibits side reactions on the anode surface. Li|LFP assembled with P(VC–PETEA)–AlF_3 has a discharge capacity of 150.4 mA h g^{-1} with a higher capacity retention (CR) of 95.4% (400 cycles, 0.5C) which is far better than that with P(VC–PETEA) with a capacity of 118.0 mA h g^{-1} and CR of 76.8%. Meanwhile, the first cycle coulombic efficiency (CE) of the Li|LFP pouch batteries with P(VC–PETEA)–AlF_3 is enhanced from 69.1% to 97.3% because of the excellent SEI characteristics.

The interaction between polymer chains and components like lithium salts/solvents can also alter the solvation structure of lithium ions. Wang *et al.* used ethoxylated trimethylolpropane triacrylate (ETPTA) to *in situ* synthesize a polymer matrix (CPCE) with high polar groups C═O on the chain segment, which is beneficial for anchoring free solvent succinonitrile (SN).[34] This helps protect the Li-metal from SN attack and creates abundant AGGs and CIPs on the Li-metal interfaces, promoting the formation of anion-derived fluorinated SEIs. On the contrary, an equal mass fraction of PEO without polar groups, which are unable to anchor SN, was employed to replace ETPTA to prepare the comparative sample GPCE. Li|Cu assembled with CPECE exhibits an excellent CE of ~99.1%, which is higher than that of GPCE, indicating of good lithium metal reversibility of the fluorinated SEI. Ma *et al.* designed a main-chain fluorinated alternating SPE (Fig. 2f), which has superior compatibility with Li-metal by forming a unique 6-membered ring solvation structure that facilitates connections between lithium ions, fluorine atoms, and oxygen atoms.[22] These interactions effectively reduce the number of free dissociated $TFSI^-$ ions and lead to the generation of more CIPs and AGGs, producing anion-derived fluorinated SEIs.

Zhang *et al.* proposed a new electrolyte based on a polymer blend, referred to as Li-polymer in F diluter (LPIFD).[35] LPIFD is a blend composed of an inert fluorinated diluter polymer (PVDF–HFP) and a lithium conduction polymer: PPC or poly(bis(trifluoroethoxy)phosphazene) (PTFEP). PPC–LPIFD is a phase-separated structure, which has poor adjustment of lithium ion solvation structure, causing dendrites to grow at phase boundaries. On the contrary, PTFEP–LPIFD can be perfectly miscible. The single-phase PTFEP–LPIFD lacks phase boundaries, which facilitates uniform lithium deposition. The addition of the fluorinated diluter polymer reduces interactions between the lithium conduction polymer and lithium ions, resulting in more CIPs and AGGs that promote LiF-rich SEI formation. Therefore, the critical current density (CCD) of PTFEP–LPIFD is 3.7 mA cm^{-2} (>0.3 mA cm^{-2} of PPC–LPIFD) and Li|NCM811 assembled with PTFEP–LPIFD had a superior cycle life of >400 cycles (CR of 80%) at 0.5 C and 4.5 V with a high average CE of 99.95%.

Solvent derived fluorinated SEIs. Fluorinated solvents in SPEs introduce fluorine groups to construct solvent-derived fluorinated SEIs. Fluoroethylene carbonate (FEC) is a notable fluorinated solvent used to create robust fluorinated SEIs among various cyclic and acyclic carbonates.[36] FEC has a lower LUMO level compared to non-fluorinated solvents (Fig. 2b), making it more prone to decomposition on the surface of lithium metal, which in turn produces a protective SEI. The addition of FEC results in an SEI that is smoother and denser compared to the SEI formed with the non-fluorinated solvent EC (Fig. 3a).[37,38] During the formation of the FEC-induced SEI, the C–F bond breaks first, producing LiF and vinylene carbonate (VC), followed by the reduction of VC. Michan *et al.* have demonstrated that the majority of lithium is consumed in the formation of LiF, with only small amounts of $Li_2C_2O_4$, HCO_2Li and Li_2CO_3 generated later, as evidenced by ^{19}F and ^{7}Li solid-state nuclear magnetic resonance (NMR) spectroscopy. In contrast, VC degradation produces large quantities of $Li_2C_2O_4$, HCO_2Li and Li_2CO_3.[39]

Studies have shown that the polymer skeleton in the SPE can regulate the solvation structure of lithium ions and induce FEC to form a uniformly deposited SEI on the surface of lithium metal. Chen *et al.* utilized polyfunctional

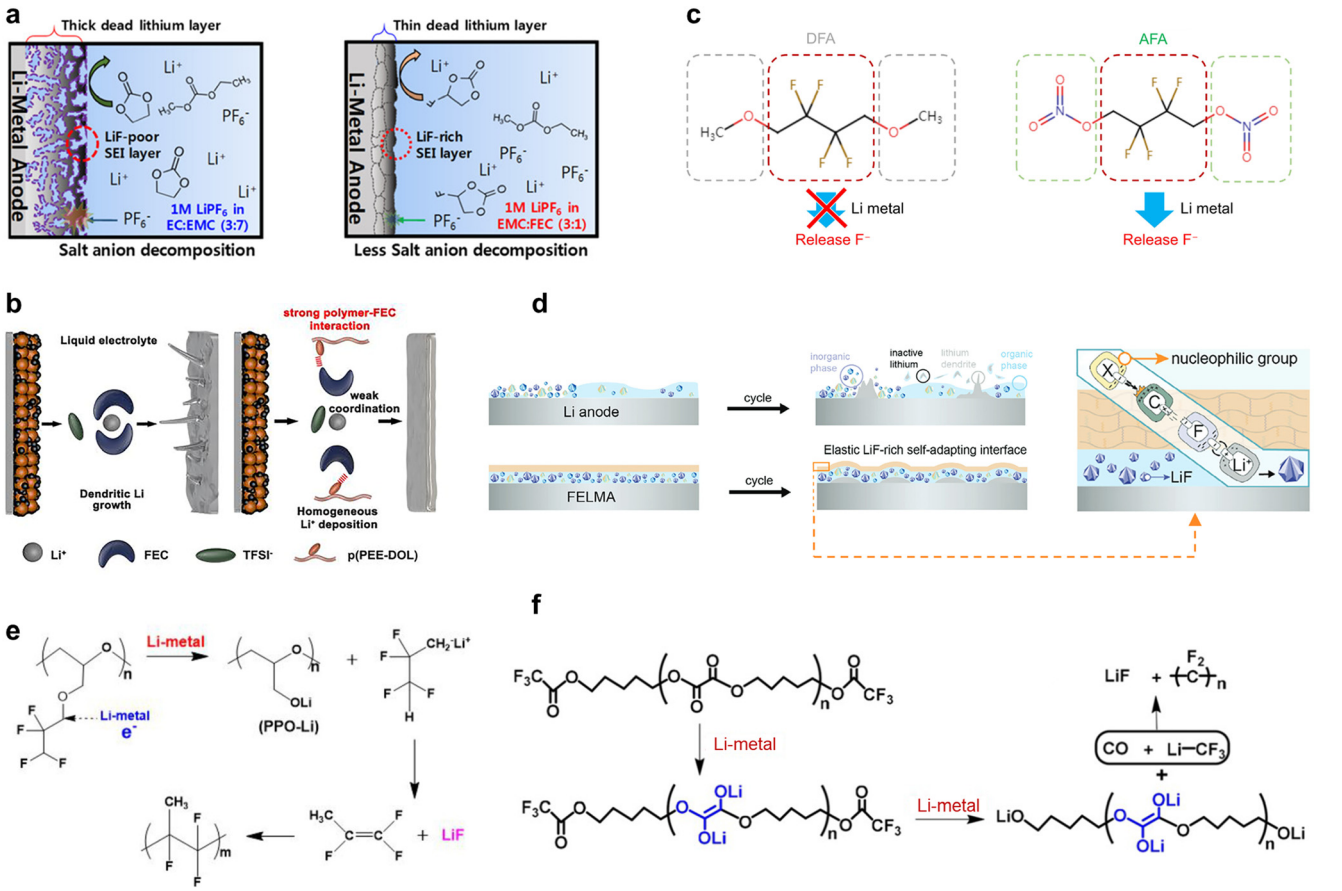

Fig. 3 Mechanism of solvent-derived fluorinated SEIs. (a) Non-fluorinated SEI derived from EC/EMC-based solvent *vs.* fluorinated SEI derived from FEC/EMC based solvent. Reproduced with permission.[37] Copyright 2018, American Chemical Society; (b) schematic illustration of desolvation mechanisms in p(PEE–DOL). Reproduced with permission.[40] Copyright 2023, Elsevier; (c) molecular design of DFA with inert methoxyl and AFA with an active nitrate ending group on the side of the fluorocarbon segment. Reproduced with permission.[41] Copyright 2022, John Wiley and Sons; (d) reaction mechanism of *in situ* formation of LiF by the PF monomer in the MG–PF–PU polymer. Reproduced with permission.[42] Copyright 2024, John Wiley and Sons; (e) reaction mechanism of TFP-containing polymers with Li-metal. Reproduced with permission.[43] Copyright 2022, John Wiley and Sons; (f) reaction mechanism of C5–POE–F with Li-metal. Reproduced with permission.[44] Copyright 2021, John Wiley and Sons.

pentaerythritol glycidyl ether (PEE) and DOL to fabricate a crosslinked GPE (c-GPE).[40] With the addition of FEC solvent up to 91 wt%, the IC of c-GPE expanded to 2.36 mS cm^{-1} at RT. However, a high proportion of FEC solvent in the liquid electrolyte system might strongly coordinate with Li^+, leading to a higher desolvation barrier and increasing the local charge-transfer impedance, consequently causing the growth of lithium dendrites in a tip-driven manner. DFT calculations of the interaction between FEC solvent and polymer matrix p(PEE–DOL) revealed that the binding energy of FEC–p(PEE–DOL) (−0.29 eV) was higher than that of the FEC–PP membrane (−0.065 eV), indicating that the polar groups from the polymer matrix p(PEE–DOL) could strongly anchor FEC solvent molecules (Fig. 3b). Thus, the introduction of p(PEE–DOL) reduced the desolvation energy in c-GPE by 26% compared to the liquid electrolyte (b-LE, 1 M $LiPF_6$ in EC/DEC), enabling a much more homogeneous fluorinated SEI from FEC. The Li|Li symmetrical battery assembled with c-GPE has run for 2800 h at 0.5 mA cm^{-2} with polarization of 15.2 mV, which is better than that of b-LE (<1200 h). Li|NCM622 assembled with c-GPE has a discharge capacity of 150 mA h g^{-1} with a higher capacity retention (CR) of 79% (300 cycles, 0.2C) which is far better than that with b-LE.

To enhance the reactivity of the C–F bond in fluorine-containing solvents, Xie *et al.* proposed a design principle for fluorinated molecules. They showed that an active ending group, $–NO_3$, attached to the β-side of the C–F bond significantly improves the reactivity of the fluorinated bond, promoting the release of fluorine and the formation of LiF on lithium metal. Conversely, 2,2,3,3-tetrafluoro-1,4-dimethoxybutane (DFA) with an inert $–OCH_3$ ending group is unable to initiate C–F cleavage (Fig. 3c).[41]

Fluorinated chain segments in SPEs provide fluorine groups to build solvent-derived fluorinated SEIs. For instance, Wang *et al.* synthesized an SPE (MG-PF-PU) containing the fluorinated monomer 3,3,4,4,5,5,6,6,6-nonafluorohexyl methacrylate (PF).[42] The strong nucleophilic groups can attack and break the C–F bonds of PF, while the strong electrophilic lithium ions combine with fluoride anions to generate inorganic LiF *in situ* (Fig. 3d). The

abundant inorganic species formed *in situ* play a crucial role in accelerating ion transport at the interface and enhancing its stability. However, excessive inorganic species cannot withstand significant volume fluctuations of the electrode due to the weak interaction forces between them. Therefore, highly viscoelastic polyurethane methacrylate (PU) was introduced. PU can participate in copolymerization through its terminal double bonds to form a cross-linked structure, anchoring the inorganic particles in place and accommodating localized uneven deposition. As for Li|NCM811 assembled with MG–PF–PU with an *N*/*P* ratio of 2.17 and *E*/*C* ratio of 2.68 g A h^{-1}, the CR can still reach 80% after 320 cycles at 0.2C/0.5C, 4.3 V, which is 200% longer than the one without MG–PF–PU.

Li *et al.* used 3-(2,2,3,3-tetrafluoropropoxy)-1,2-propylene oxide (TFP) to construct a fluorine-containing polymer.[43] XPS data indicated that the degradation of TFP-containing polymer chains produced LiF and PPO-Li species, which *in situ* formed a composite SEI layer to passivate the interface (Fig. 3e). Sun *et al.* utilized poly-oxalate with trifluoroacetate-terminated segments (C5–POE–F) as an electrolyte.[44] XPS was conducted to study the degradation mechanism of the C5–POE–F electrolyte on the lithium metal surface. After cycling in a Li|Li symmetrical battery, the C–C signal in the XPS

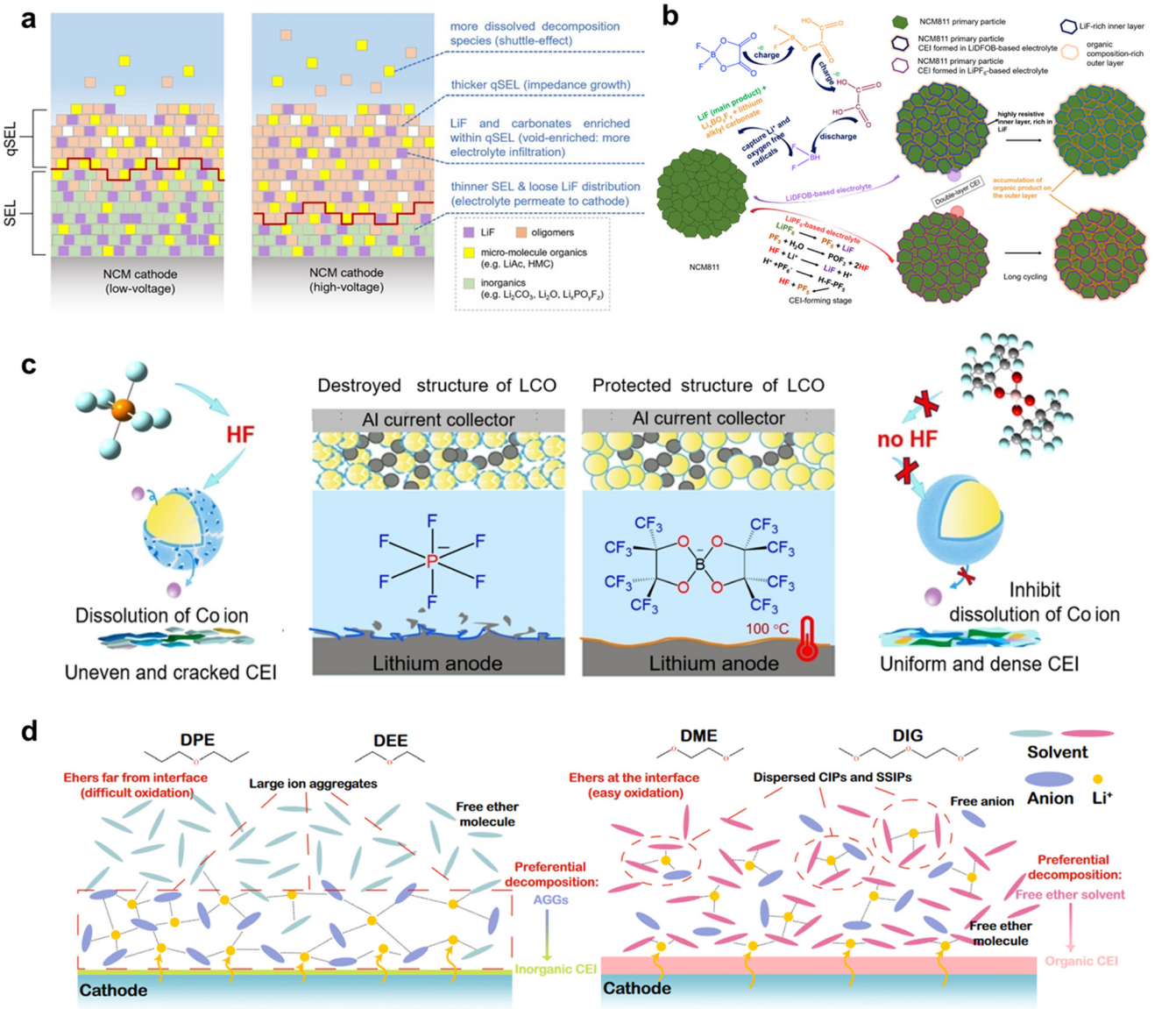

Fig. 4 Formation mechanism of fluorinated CEIs. (a) Architecture comparation of CEI layers formed at low/high voltage. Reprinted with permission.[48] Copyright 2023, American Chemical Society; (b) scheme of CEI formation and revolution on the NCM811 cathode using LiDFOB and $LiPF_6$ based electrolytes during cycling. Reprinted with permission.[49] Copyright 2020, Elsevier; (c) schematic illustration of the positive role of LiFPB salt in protecting the LCO cathode and lithium anode. Reprinted with permission.[50] Copyright 2024, John Wiley and Sons; (d) illustrations of the interfacial model of weakly solvated ether electrolytes and polar ether electrolytes at the NCM cathode surface. Reprinted with permission.[51] Copyright 2023, Springer Nature.

spectrum became asymmetrical and shifted to 284.4 eV, indicating the generation of C=C bonds. The C–O signal slightly intensified, suggesting an increase in C–O content after cycling. Additionally, a LiF signal was observed after the interfacial reaction, confirming the degradation of oxalate units and terminal CF_3–CO groups to form lithium enolate and LiF species, respectively, which together create a composite SEI passivation layer (Fig. 3f).

2.2. Mechanism of fluorinated electrolytes affecting formation of CEIs

High voltage cathodes are crucial for enhancing the energy density of LMBs. Achieving a higher working voltage allows for greater energy storage in a single battery, thereby increasing the overall energy density of LMBs. However, as the cut-off voltage increases, the instability of the high voltage cathode itself and the CEI can significantly reduce its lifespan.[45–47] Currently, the mainstream model for CEI structure is considered to be a bilayer model. This three-dimensional bilayer model consists of an inner solid electrolyte layer (SEL) made of dense inorganic species and a gel-like outer quasi-solid electrolyte layer (qSEL) composed of a polymer network.[47,48] The SEL primarily comprises complete decomposition products of solvents and salts, such as oxides and fluorides, while the qSEL consists mainly of incomplete decomposition products like polyolefins, semicarbonates, and polymers. To characterize the microstructure of the CEI, researchers often use a typical "wash-then-test" method, which can damage the qSEL and lead to misunderstandings of the CEI structure. To address this, Luo *et al.* developed a comprehensive characterization approach that combines Fourier transform infrared spectroscopy, solution NMR, XPS, and mass spectrometry. This method allowed for the reconstruction of the original CEI layer model.[48] Their findings revealed that high voltage exacerbates electrolyte decomposition, leading to the thickening of the qSEL (Fig. 4a). LiF species are distributed within the relatively unstable qSEL, resulting in a weaker CEI. Additionally, the thinner SEL exhibits high porosity, making it susceptible to electrolyte soaking. This condition can further thicken the qSEL and increase the battery's impedance, ultimately causing a significant degradation in the capacity of the high voltage battery.

The current approach to improving the CEI between high voltage cathodes and electrolytes primarily focuses on modifying the electrolyte components in SPEs. For example, adding fluorinated lithium salts and additives into SPEs can promote the formation of a robust CEI, and using antioxidant solvents can significantly expand the ESW of SPEs.[52] One effective lithium salt is LiDFOB, which combines the advantages of $LiBF_4$ and lithium bis(oxalate)borate, offering better chemical and electrochemical stability than the commonly used $LiPF_6$. LiDFOB is preferentially oxidized, forming a denser and more resistive CEI than $LiPF_6$ and carbonate solvents.[49] During CEI formation, $DFOB^-$ anions are reduced to B–O bonds and oxalate rings, generating oxygen and $-BF_2$ radicals that capture solvent molecules. This results in an inner resistive LiF-rich layer and an outer organic-type $Li_xBO_yF_z$ CEI layer on the high voltage nickel-rich cathode. Consequently, a uniform and dense CEI forms on the surface of the NCM811 cathode, protecting it from damage. In contrast, $LiPF_6$-based electrolytes form CEIs containing more LiF but are sensitive to water, which can react to form corrosive HF. This issue does not occur with $DFOB^-$ anions (Fig. 4b). Although $LiPF_6$-based electrolytes create more LiF, LiDFOB-based electrolytes form denser hierarchical CEIs. These CEIs protect the high-voltage cathode from electrolyte erosion, inhibit further electrolyte decomposition, and prevent the accumulation of organic products in the outer CEI layer during long cycling processes. They also inhibit the overgrowth of charge-transfer impedance. Another lithium salt, lithium perfluoropinacolatoborate (LiFPB), offers excellent thermal and electrochemical stability without generating corrosive HF gas at high temperatures and pressures (Fig. 4c). Similar to LiDFOB, LiFPB-based electrolytes can form a protective CEI with an organic outer layer and an inorganic inner layer on the surface of $LiCoO_2$ electrodes. Additionally, LiFPB serves as a bifunctional lithium salt that enhances the stability of the anode–electrolyte interface by forming a phase with high IC on the lithium anode. This is due to the FPB-anions' tendency to integrate into lithium-ion solvated structures, creating a LiB_xO_y-based SEI.[50] Heptafluorobutyric anhydride (HFA) is a tetrafunctional additive whose reductive and oxidative decomposition promotes the formation of a homogeneous inorganic-rich SEI and a dense CEI. It optimizes lithium-ion solvation for stable lithium deposition/degradation and acts as a surfactant to enhance electrolyte wettability on the membrane, improving lithium-ion flux. Batteries containing HFA maintain a smooth CEI interface without breakage or swelling after cycling. XPS analysis indicated reduced dissolution of transition metals due to the dense CEI's protection, while increased LiF content ensured rapid Li^+ transport within the CEI layer, extending the high-voltage battery's lifespan.[53]

Simultaneously, the concept of "salt-in-solvent" is also valuable for constructing fluorinated CEIs. HCEs and DCEs significantly reduce the number of free solvent molecules and increase the amount of AGGs and CIPs, which are beneficial for enabling anion-derived fluorinated CEI formation on cathodes.[54] For instance, Jiang *et al.* reported ether-based DCEs with low concentrations of fluorinated fluorobenzene (FB) as a diluent.[55] The addition of FB greatly reduces the decomposition of DME by enhancing the interactions between DME, FSI^-, and Li^+, thereby boosting the content of LiF species. Choi *et al.* demonstrated that a DCE containing 1,2-difluorobenzene can effectively improve the cycle stability of high-voltage LMBs.[56] Additionally, Zhang *et al.* found that 1,3,5-trifluorobenzene (3FB) synergized with FB can enhance the thermodynamic and interfacial stability of DCEs.[57] This synergy significantly reduces defluorination,

leading to less HF generation and the formation of a durable, thin LiF-rich protective film on the interphase of high-voltage cathodes, balancing electrochemical performance and long-term cycling stability. Beyond adding fluorinated diluents, the electrode/electrolyte interface can be kinetically stabilized by rearranging the degradation of solvent species in the electrolyte and modulating the cathode surface bilayer composition. Li *et al.* reported a dilution strategy to modify the interactions between Li^+ and the solvent by exploiting the low viscosity and surface tension of dipropyl ether. This strategy facilitates the migration of AGGs to the cathode surface, repelling the free ether molecules and preventing them from coming into direct contact with the cathode surface, thereby mitigating their oxidation (Fig. 4d). XPS analysis shows that this strategy induces the formation of more LiF-containing CEIs, ensuring the stability of the high-voltage cathode.[51] These approaches illustrate the potential of "salt-in-solvent" strategies to construct robust, fluorinated CEIs that enhance the performance and longevity of high-voltage LMBs. By carefully selecting and combining electrolyte components, researchers can significantly improve the stability and efficiency of these advanced battery systems.

2.3. Advanced characterization techniques for understanding LiF-rich interphases

To design SEIs/CEIs that are more electrochemically stable, robust, and rich in LiF components, it is crucial to thoroughly understand their morphology, nanoscale structure, chemical composition, and mechanical properties. However, characterizing these interphases presents significant challenges due to several reasons: (1) complex compositional structure: SEIs/CEIs consist of various components, including electrolyte components and products generated from interfacial reactions. (2) Multiple coupled reaction effects: interactions among different reactions cause the physicochemical properties of SEIs/CEIs to evolve over time. (3) Extremely thin interface layers: SEIs/CEIs are very thin, requiring high-resolution techniques for detailed structural and compositional analysis. (4) Influence of operating conditions: operating conditions such as temperature, current density, and cycle number significantly impact the structure and performance of SEIs/CEIs, increasing the complexity of both static and dynamic characterization.[49,58–60] Therefore, powerful characterization tools are essential for understanding SEIs/CEIs and guiding the design of more robust SEIs/CEIs to enhance battery performance. This section summarizes recent literature reports on advanced techniques for detecting SEIs/CEIs, providing readers with insights into the most cutting-edge methods used in the field.

Morphology & nano structure. The morphological structure of electrode materials is typically characterized using scanning electron microscopy (SEM) and transmission electron microscopy (TEM) techniques. However, *ex situ* SEM and TEM methods cannot provide key information about dynamic processes occurring during battery operation or require complete disassembly of the battery, which may damage the surface layer and expose reactive surface materials to glove box atmosphere, potentially altering the observed substances even with minimal contamination. In contrast, *in situ* SEM and TEM have the potential to capture dynamic processes occurring within very small time scales (~ms or shorter) during electrochemical system operation, allowing for a better understanding of these specific processes.

Golozar *et al.* used *in situ* SEM to dynamically characterize the interface between the SPE and lithium metal, observing the growth of lithium dendrites at the anode, opening of grain boundaries, and formation and depletion of isles on the anode surface during electrochemical cycling (Fig. 5a).[61] Gong *et al.* used *in situ* TEM to find that LiF-rich SEI can produce denser lithium structures, which are particularly prone to uniform stripping, thereby suppressing lithium detachment and separation.[62]

SEIs/CEIs are highly sensitive to oxygen, humidity, carbon dioxide, and light beam. Lithium dendrites can melt under high-dose electron radiation in conventional TEM, causing inevitable damage to the sample.[67] Additionally, the chemical properties and intermediate phases of the sample can be easily contaminated during conversion and preparation processes. Therefore, cryo-EM has been introduced into SEI/CEI research. Scientists use this advanced characterization technique to detect the crystal structure of lithium dendrites and the chemical composition of SEIs/CEIs, achieving atomic-level representation of the original morphology, chemical composition, and spatial distribution. The Cui research group was among the first to use cryo-EM to study the atomic structure of SEI films formed on the surface of metallic lithium in different electrolyte solutions.[26] Zhang *et al.* proposed a new sample preparation method specifically designed for SPE-containing lithium batteries: low-temperature ultrathin slicing (Fig. 5b),[63] enabling the production of large-scale low-temperature TEM samples to directly visualize the global SEI and lithium in the SPE from nanometer to millimeter scales. Combining electron energy loss spectroscopy with multivariate least-squares fitting, they illustrated the deposition of dead lithium clusters, revealing that lithium clusters consist of Li^0 and LiH cores surrounded by inorganic components such as Li_2O and LiOH, but with minimal LiF content, further encapsulated by organic components (Fig. 5c).

Chemistry composition. X-ray photoelectron spectroscopy (XPS) relies on photon beams to probe SEI/CEI film samples, providing relevant chemical information. Theoretically, photon beams almost do not damage the sample, making it a standard technique for characterizing SEI and CEI layers, offering rich chemical signals albeit at the expense of in-plane spatial resolution. For example, according to the F 1s XPS spectra, significantly more LiF species are formed at the interphases of Li-metal and NCM-83 in batteries assembled with the fluorinated T-SPE after 100 cycles at 1 mA cm^{-2} compared to those with the non-fluorinated E-SPE (Fig. 5d).[64] However, the SEI often exhibits a 3D structure, making it

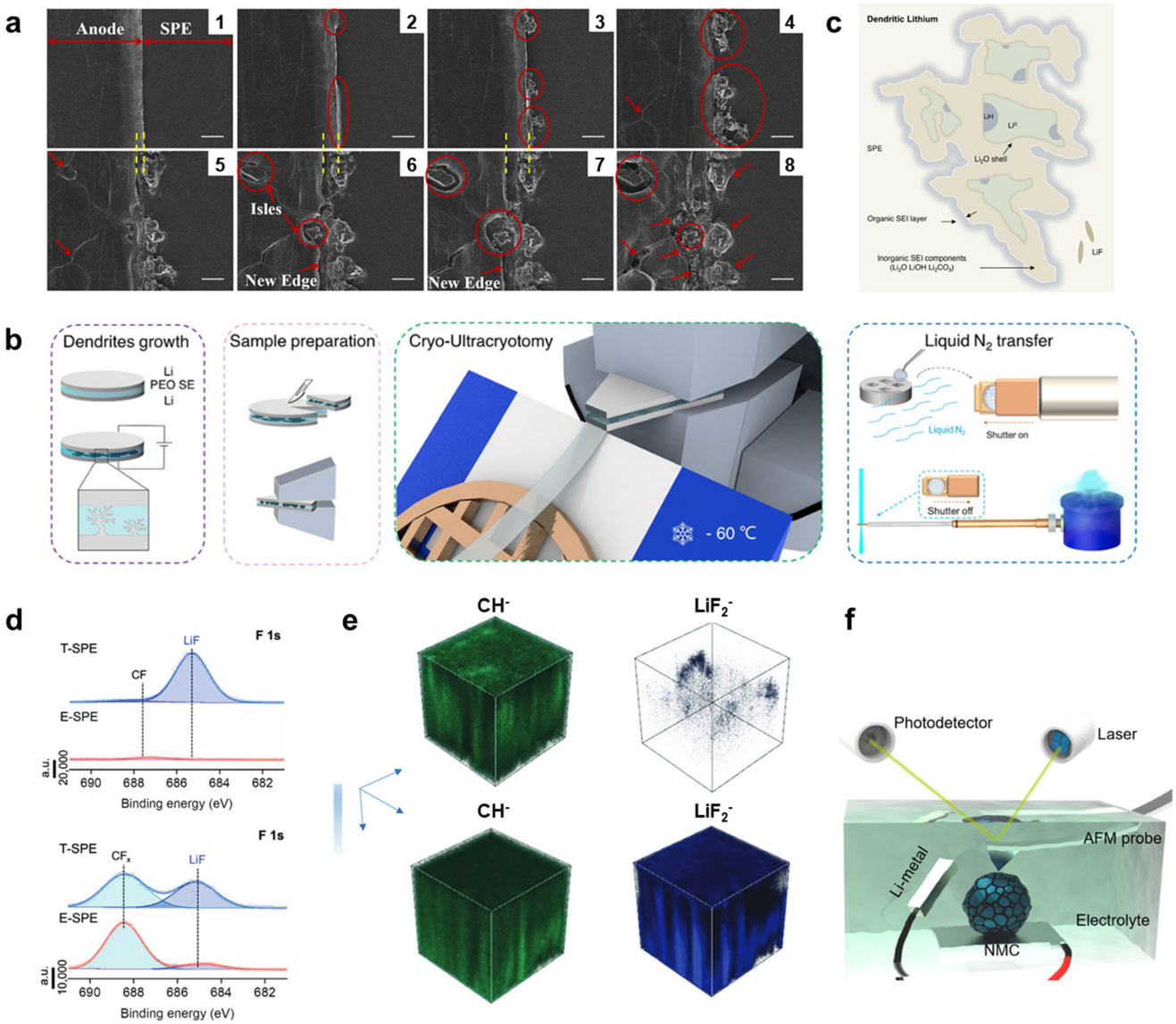

Fig. 5 Advanced characterization techniques for understanding SEIs/CEIs. (a) *In situ* cross sectional SEM of the interface between lithium anode and SPE during the cycling process. The interface evolves from state 1 to state 8. Reproduced with permission.[61] Copyright 2019, the author(s); (b) schematic for cryo-EM sample preparation: low-temperature ultrathin slicing; (c) schematic images of the structure of the lithium cluster. Reproduced with permission.[63] Copyright 2024, Royal Society of Chemistry; (d) F 1s XPS spectra of cycled Li-metal anodes (top) and cycled NCM-83 cathodes (low) using the non-fluorinated E-SPE and fluorinated T-SPE. Cycled Li-metal and NCM-83 are harvested from the battery after 100 cycles at 1 mA cm^{-2}. Reproduced with permission.[64] Copyright 2024, John Wiley and Sons; (e) ToF-SIMS depth profiles of a non-fluorinated SPE (top) *vs.* a fluorinated SPE (low). Reproduced with permission.[65] Copyright 2024, John Wiley and Sons; (f) schematic diagram of *in situ* AFM for NMC cathode materials. Reproduced with permission.[66] Copyright 2021, Elsevier.

quite challenging to achieve spatial structure analysis using only XPS.

In contrast, Time-of-Flight Secondary Ion Mass Spectrometry (ToF-SIMS) can provide 3D characterization of the component content in SEIs/CEIs. It is a highly surface-sensitive technique suitable for analyzing organic and inorganic substances with a depth resolution of up to 1 nm. ToF-SIMS provides ion mass-to-charge ratio spectra for quantitative chemical analysis, identifying known components and detecting unknown structures and contaminants with excellent isotope resolution. Additionally, it can detect ion fragments on ultra-thin films that traditional methods cannot, achieving non-destructive analysis with a single pulse to collect a complete spectrum.

ToF-SIMS is primarily used to provide depth profiles of SEI/CEI chemical compositions. Peng *et al.* characterized the SEI of fluorinated and non-fluorinated SPEs using ToF-SIMS.[65] In fluorinated electrolytes, the outer layer of the SEI film is rich in CH^- species (representing organic species) compared to LiF_2^- species (representing LiF), whereas the inner layer is richer in LiF_2^- and contains few CH^- species. This indicates that fluorinated electrolytes form an organic–

inorganic composite SEI (Fig. 5e). The outer layer of the SEI is enriched with organic structures, while the LiF-rich inner gradient layer completely covers the lithium negative electrode. This stable insulating SEI film helps prevent side reactions and lithium dendrite growth.

Mechanical properties. The interface layer (CEI, SEI) between the SPE and the electrode surface must possess sufficient toughness and elasticity to accommodate significant volume changes during battery cycling, while also having adequate strength to prevent cracking. Therefore, it is essential to focus on the mechanical properties of these interface layers and their impact on battery cycling performance. Atomic Force Microscopy (AFM), a precise evaluation technique based on molecular interactions between the probe and the sample, can measure various physical properties of samples, including height, mechanical strength (mechanical microscopy), and conductivity (conductive microscopy).[68,69] Notably, AFM can be easily integrated with *in situ* battery setups as it does not require a vacuum environment (Fig. 5f).[66] Researchers commonly use AFM to probe the mechanical properties of SEIs and CEIs.

A high elastic modulus of interphases is beneficial for the cycling performance of LMBs. On the SEI side, Shen *et al.* proposed that a high elastic modulus above 3 GPa can achieve stable cycling of LMBs.[70] Yoon *et al.* confirmed that a higher CE can be obtained when the elastic modulus of SEI is 4.6 GPa.[71] Zhang *et al.* used *in situ* AFM to confirm that transition metal cations migrating from the cathode degrade the mechanical performance of the SEI. Mn^{2+} induces the formation of thick, soft, and unstable SEI layers, reducing the SEI modulus from 18 GPa to approximately 1 GPa. In contrast, Ni^{2+} and Co^{2+} were observed to increase the accumulation of the SEI at the edge and basal planes, reducing the SEI modulus from 18 GPa to 5 GPa. These factors drive battery capacity loss and instability. Zhang *et al.* found that the SPE formed *in situ* on the surface of lithium metal improves the mechanical performance of the SEI.[72] *In situ* AFM revealed that the average Derjaguin–Müller–Toporov (DMT) modulus of the SEI formed *in situ* before lithium deposition was approximately 2.9 GPa, about 2.1 times that of the liquid-state group. After lithium deposition, the average DMT modulus of the SEI of the *in situ* polymerized group on the working lithium anode was 3.6 GPa, six times that of the liquid-state group SEI's DMT modulus (0.6 GPa).

On the CEI side, *in situ* AFM can reveal the mechanical properties and interface evolution of the CEI. For example, researchers monitored the dynamic formation of the CEI on high-Ni positive electrode materials between GPEs using *in situ* AFM, providing valuable insights into the unique nanoscale structure and growth dynamics of the LiDFOB-mediated CEI on $LiNi_6Co_2Mn_2O_2$ cathodes. And the GPE *in situ* formed on the surface of the CEI also can improve the mechanical strength of the CEI.[73] Lu *et al.* found that the CEI on $LiCoO_2$ forms only at the edge plane under high pressure, with no formation observed at the basal plane.[74] Chen *et al.* used electrochemical AFM (EC-AFM) to discover that a dense CEI was not observed on the surface of lithium-rich and manganese-rich (LMR) cathode materials in carbonate

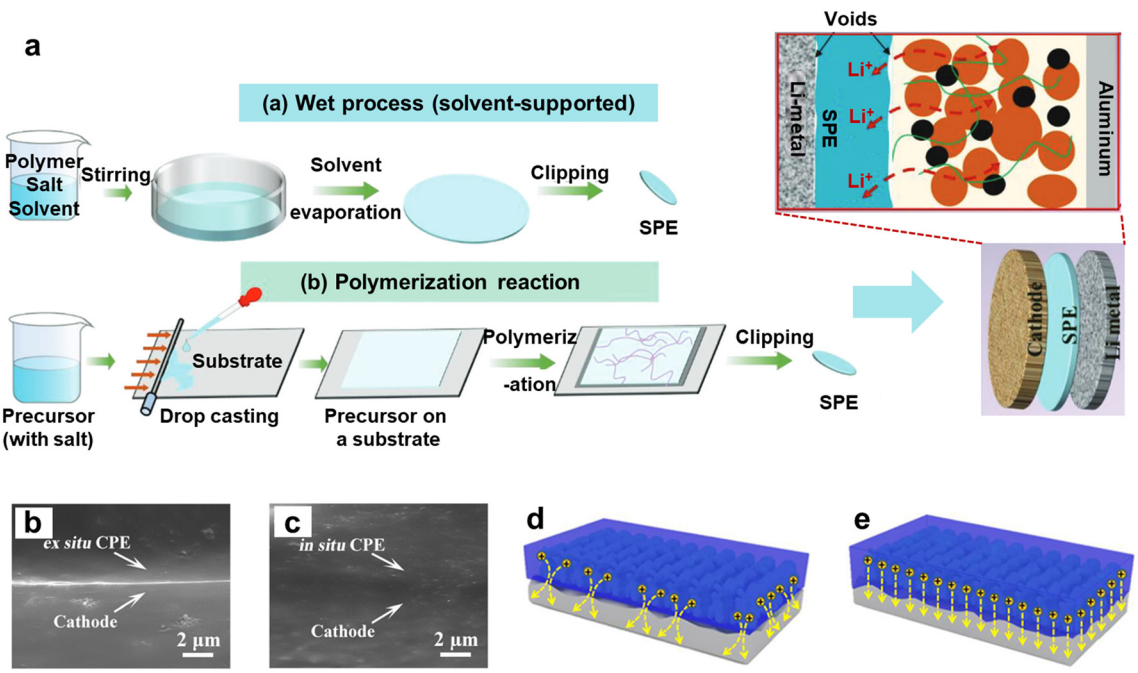

Fig. 6 (a) *Ex situ* polymerization route for preparing SPEs. Reproduced with permission.[5] Copyright 2023, John Wiley and Sons; (b) impact of *in situ* polymerization *vs. ex situ* polymerization; cross-sectional images of the interface between the *ex situ* CPE and cathode (b) *vs. in situ* CPE and cathode (c); schematic illustration of Li-ion transport at (d) the *ex situ* CPE||cathode interface and (e) *in situ* CPE||cathode interface. Reproduced with permission.[78] Copyright 2020.

electrolytes. In contrast, after injecting fluorine-rich electrolyte (1 M $LiPF_6$ FEC/FEMC /HFE), significant morphological changes were observed on the LMR at high voltage. At 4.6 V, a uniform, dense, and lamellar SEI layer was observed, and the morphology remained relatively stable afterward.[75]

3. Manufacturing strategies for SPEs

3.1. *Ex situ* polymerization

The preparation process of *ex situ* polymerization is relatively complex. Currently, the preparation of SPEs *via ex situ* polymerization can primarily be achieved through two methods (Fig. 6a). The first method, a wet process, involves dissolving pre-synthesized polymers (such as PEO, PVDF, *etc.*) and lithium salts into a low-boiling-point solvent (*e.g.*, DMF, AN, *etc.*) to form a homogeneous solution. This solution is then uniformly poured into a glass dish and placed in a convection oven to allow the solvent to evaporate completely, resulting in a dry SPE.[76,77] The second method, polymerization reaction, involves mixing lithium salts, monomers, and a suitable initiator to form a precursor solution. This precursor solution is then cast into a mould, and after thermal or photoinitiation, a polymerization reaction occurs, producing the SPE.[11] The SPEs obtained by these two methods can be directly used as support membranes in battery assembly by placing them between the anode and cathode without the need for an additional membrane. However, SPEs prepared *via ex situ* methods generally exhibit poor solid–solid interfacial compatibility with electrodes and high interfacial impedance. This issue arises because the cathode is typically a porous material structure, containing small voids between the carbon black and active materials. Liquid electrolytes can effectively infiltrate these pores, facilitating rapid ionic conduction between the active materials and carbon black. Although *ex situ* polymerized SPEs possess a certain degree of flexibility, they still struggle to fully infiltrate all the active materials within the cathode, leading to poor interfacial compatibility between the active materials and the SPE, and consequently, low IC across the interface. Additionally, the *ex situ* preparation process is cumbersome, with solvents used in the wet method being harmful to the environment and human health, which is not aligned with current green and sustainable development strategies.

3.2. *In situ* polymerization

Compared to *ex situ* polymerization, the electrolyte generated by *in situ* polymerization can achieve better solid–solid interfacial compatibility. Qin *et al.* found that by thoroughly wetting the electrodes and filling the pores within them before polymerization, the SPE formed after polymerization can make good contact with the electrodes. The overall resistance of the *in situ* SPE/electrode assembly was reduced by nearly eight-fold compared to *ex situ* SPEs, primarily due to the reduction in interfacial resistance.[79] As shown in the cross-sectional diagram of the cathode and SPE (Fig. 6b and c), there are visible gaps between the *ex situ* SPE and the cathode, while no such gaps exist between the *in situ* SPE and the cathode, indicating good adhesion between the *in situ* SPE and the cathode material. Moreover, a well-adhered interface facilitates more uniform and rapid ionic conduction, in contrast to interfaces with larger gaps, where ionic conduction is uneven (Fig. 6d and e). Uneven ionic conduction on the surface of lithium metal can lead to the formation of tip effects,[80] which may result in lithium dendrite growth and reduced battery capacity.

Currently, the mainstream method for *in situ* polymerization to prepare SPEs is the separator-assisted method. In this method, lithium salts, monomers, and a suitable initiator are mixed to form a homogeneous precursor solution, which is then directly injected into the separator placed between the anode and cathode. The precursor solution fully infiltrates the pores within the separator and the surfaces of the electrodes. Subsequently, the precursor solution within the assembled battery undergoes *in situ* polymerization on the surfaces of the anode and cathode, forming an SPE with continuous ionic pathways (Fig. 1).[81] This method is simple to operate and can be integrated with the current "roll-to-roll" manufacturing process used in battery production. To employ this preparation method, the polymerization reaction typically needs to be initiated by heat or at RT.

It is worth noting that the choice of membrane in this supported membrane assisted method is very important. Generally, the support membranes commonly used in this process can be categorized into polyolefin and non-polyolefin membranes. Polyolefin membranes, such as polypropylene (PP) and polyethylene (PE), are widely used due to their low cost and large-scale commercial applications, but they might have poor wettability with certain fluorinated and cyano-based monomers. Non-polyolefin membranes, such as glass fiber, offer better liquid wettability and are therefore widely used. However, the mechanical properties of these two types of membranes remain unsatisfactory. In order to further enhance the mechanical properties of membranes, researchers modify the material/structure of the support membrane. For instance, Qin *et al.* employed meltblown cloth to enhance the mechanical strength of the fluorinated SPE.[82] The precursor liquid fully infiltrated the meltblown cloth framework, forming a dense and compact polymer membrane. The introduction of meltblown cloth increased the fracture strength of the fluorinated SPE from 0.025 MPa to 1 MPa. Yang *et al.* used electrospinning technology to fabricate a SiO_2NF support membrane using tetraethyl orthosilicate and poly(vinyl alcohol), thereby improving the overall mechanical properties of the SPE.[83] SPEs with higher mechanical strength can be made thinner, which in turn enhances IC and increases battery energy density. Moreover, the high mechanical strength of SPEs can improve battery safety by preventing short circuits and inhibiting the growth of lithium dendrites. Newman and Monroe have predicted

that a rigid solid-state electrolyte membrane with a shear modulus $G' > 7$ GPa can effectively suppress lithium dendrite growth.[84] Meng *et al.* have conducted a series of studies developing a strategy for pressure-tailored lithium deposition. By increasing the stack pressure in lithium metal batteries, they achieved dense and uniform lithium deposition.[85] Therefore, the cycling degradation and safety issues of lithium anodes can be mitigated through mechanical blockage.

Furthermore, some research has documented the application of photoinitiated *in situ* polymerization reactions. This technique entails the discrete application of a precursor solution to the anode and cathode surfaces. Upon complete wetting of the electrodes, photoinitiation is employed to form an SPE on each electrode surface, which is then assembled into the battery.[82] This suggests that the method could be classified as a variant of semi-*in situ* polymerization, given that *in situ* polymerization occurs independently on the anode and cathode surfaces. While this method effectively addresses the challenge of poor solid–solid interfacial compatibility between the SPE and the electrodes, it does not ensure the formation of continuous ionic pathways throughout the bulk of the SPE. The impact of this on the electrochemical performance of the battery remains an open question. Consequently, section 4.2 will focus primarily on fully *in situ* polymerization methods, specifically the separator-assisted approach.

4. Current progress of *in situ* polymerization based on fluoromonomers

In this section, we focus on the process of *in situ* polymerization involving fluoromonomers. We will discuss how initiators and fluoromonomers affect the *in situ* polymerization process, which may further influence the properties of SPEs, including electrochemical stability, interfacial stability, mechanical performance, battery cycle life, thermodynamic stability, *etc.* The development of *in situ* fluorinated SPEs will be explored based on different polymerization mechanisms, namely ionic polymerization (*e.g.*, cationic ring-opening polymerization (ROP) and anionic ROP) and free radical polymerization. For ionic polymerization, monomers will be discussed according to the number of rings (*e.g.*, ternary rings, quintuple rings, *etc.*). For free radical polymerization, monomers will be categorized by types (*e.g.*, acrylates, vinylidene carbonate system) to facilitate easier reading and understanding for the reader.

4.1. Ionic polymerization

Ion polymerization can initiate the polymerization of olefin monomers and cyclic monomers. However, since there are currently no reports on the *in situ* polymerization of fluorinated olefin monomers initiated by ions in batteries, this section mainly focuses on ion-initiated *in situ* ROP of fluorinated cyclic monomers. Mechanistically, with the exception of a few ROPs that follow a stepwise mechanism (such as ring-opening metathesis polymerization (ROMP)),[86] the majority of ROPs proceed *via* a chain-growth ionic polymerization mechanism. The polymerization mechanism of ROP can be categorized based on the type of initiator used. Initiators commonly used in the ionic polymerization of olefin monomers can also be employed in ROP. However, the anionic active species in ROP are often oxyanions (~O–A+), thioanions (~S–A+), or amine anions (~NH–A+), while the cationic active species are typically oxonium ions (≡O+B–) or sulfonium ions (≡S+B–).[87] Essentially, whether an ROP proceeds through an anionic or cationic mechanism depends on whether the atoms in the monomer are more susceptible to attack by an anionic initiator (corresponding to anionic ROP) or a cationic initiator (corresponding to cationic ROP).

4.1.1 Anionic ROP. Traditional initiators for anionic polymerization include alkali metals (such as Li and Na), sodium alkoxide, hydroxides, amides, organometallic compounds, and alkaline earth metal oxides.[88] Typical monomers that can be initiated by anionic initiators include cyclic carbonates, cyclic anhydrides, cyclic amides, and others. These monomers are essential for developing SPEs with desirable properties for high-performance batteries. By selecting appropriate initiators and monomers, researchers can tailor the polymerization process to achieve specific structural and functional characteristics in SPEs, thus enhancing their suitability for various applications in energy storage.

Ternary rings. Researchers have found that using sodium methoxide as an initiator leads to the anionic ROP of highly reactive ethylene oxide, resulting in PEO polymers with high molecular weights (MW) (30 000–40 000 g mol^{-1}) and narrow PDI.[89] In contrast, under the same conditions, propylene oxide yields PEO polymers with lower MWs (3000–4000 g mol^{-1}) due to the ease of hydrogen atom on methyl group transfer in the propylene oxide monomer.[90] For salt-doped PEO (Mn = 20 kg mol^{-1}), IC exceeding 1 mS cm^{-1} is observed only above 90 °C, where the storage modulus falls below 10 Pa.[91] This reduction in IC is attributed to the dense polymer chain structure formed by the high MW PEO, which limits ion mobility within the material.[92] However, the robust polymer chain network formed by higher MW PEO provides better mechanical support and strength, enhancing the material's mechanical properties. Therefore, selecting an appropriate initiator to control the MW of the cyclic ether reaction is crucial.

Dreier and colleagues synthesized a conductive polymer carrying fluorinated anion functional groups (Mn = 15.1 kg mol^{-1}, D = 1.09) (Fig. 7a) by combining activated carbon anions, anionic ROP, and Mitsunobu reaction. Compared to the PS-*b*-PEO-based SPE, this conductive polymer exhibits significantly improved IC and lithium-ion transference number.[93] Alexander and colleagues employed direct monomer activation *via* anionic ROP of glycidyl propargyl ether to obtain a click-functionalized polyether backbone

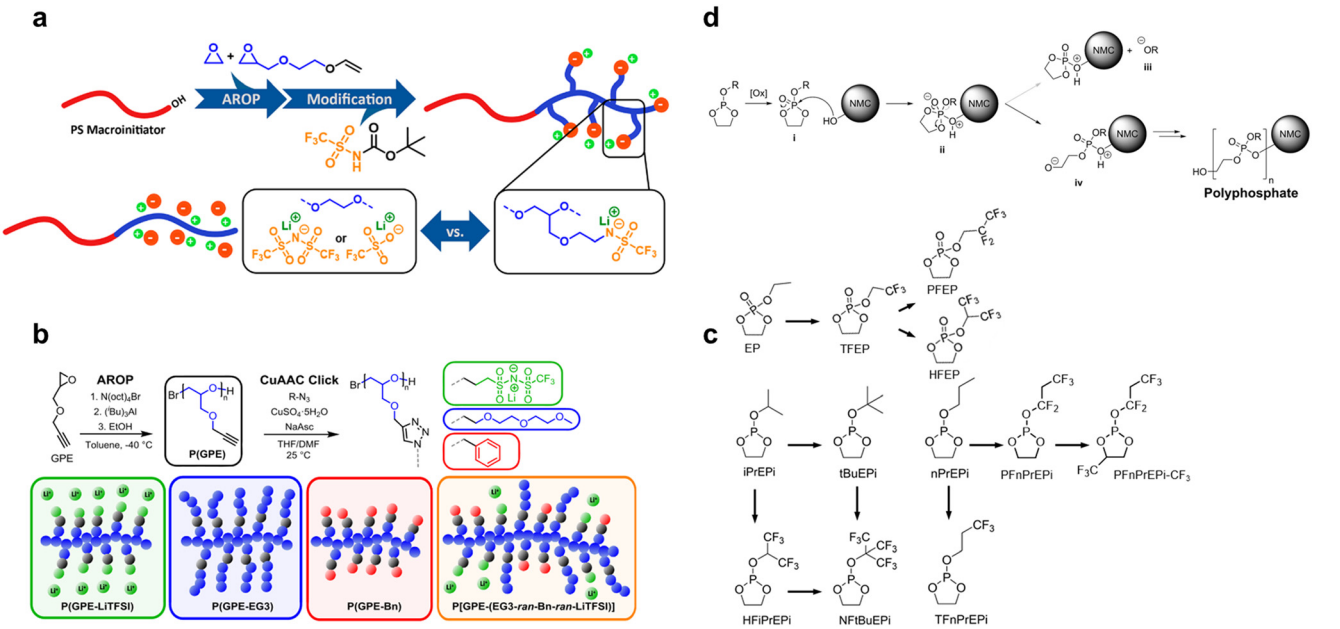

Fig. 7 Copolymerization with fluorinated monomers *via* anionic ROP. (a) Synthesis routes of a single-ion fluorinated copolymer electrolyte *via* anionic ROP. Reproduced with permission.[93] Copyright 2022, American Chemical Society; (b) synthesis routes of a single-ion fluorinated copolymer electrolyte *via* anionic ROP and click chemistry. Reproduced with permission.[94] Copyright 2019, American Chemical Society; (c) chemical structures of different fluorinated and non-fluorinated cyclic phosphate monomers; (d) schematic diagram of the formation of polyphosphates from phospholanes on the NCM cathode surface *via* anionic ROP. Reproduced with permission.[95] Copyright © 2021, John Wiley and Sons.

with high MW and narrow distribution. By incorporating fluorinated anions, benzyl, and ether oxygen functional groups onto the polymer side chains through click chemistry, they synthesized P[GPE-(EG3-ran-Bn-ran-LiTFSI)] with high electrochemical stability and a lithium-ion transference number close to 1 (Fig. 7b).[94] While both electrolyte materials demonstrate innovative structural designs, their complex synthesis pathways and lack of practical validation in solid-state electrolyte batteries remain as challenges.

Quintuple rings. Researchers have found that cyclic fluorophosphates tend to undergo *in situ* anionic ROP on the NCM cathode, due to the reason that it can be initiated by the hydroxyl groups on the surface of NCM cathode materials. Some cyclic fluorophosphate monomers currently reported in the literature are shown in Fig. 7c. The phosphorus centre of the cyclic fluorophosphate can be nucleophilically attacked by hydroxyl groups abundant on the surface of the cathode active material (NCM-OH), leading to proton transfer and the formation of a protonated intermediate. The presence of acid in the electrolyte can further facilitate this step, making the cyclic phosphate more susceptible to nucleophilic attack. This unstable intermediate undergoes another proton transfer step, causing the cyclic phosphate to undergo a ROP (Fig. 7d).

Su *et al.* have theoretically shown that non-fluorinated monomers, such as EP, can undergo the same reaction.[96] In comparison, the presence of an electron-withdrawing $-CF_3$ substituent in fluorinated monomers like TFEP makes the phosphorus in the –P═O group more prone to nucleophilic attack by the active material, leading to easier ROP of the fluorinated phosphate. Adding 1% TFEP to 1.2 M $LiPF_6$ in EC = 3 : 7 vol% can induce *in situ* polymerization on the cathode surface to form a fluorine-containing passivation polymer. Compared to the liquid electrolyte control group without TFEP, the polymer *in situ* formed on the cathode surface significantly improved the first-cycle capacity of Gr|NCM532. The polymer formed from the anionic ROP of fluorophosphates can also enhance the performance of lithium metal batteries. Zheng *et al.* found that a precursor solution of 0.95 M LiFSI in TFEP = 1 : 3 vol% showed a good IC of 2.19 mS cm^{-1} (RT) after *in situ* polymerization on the cathode surface. Compared to the control group (1 M $LiPF_6$ in EC : DMC = 1 : 1 vol%), it exhibited better electrochemical stability (LSV: 4.9 V *vs.* 4.5 V). The Li|NCM111 battery with it also demonstrated longer cycle life, with a CR of 86.5% after 200 cycles at a cutoff voltage of 4.5 V, far exceeding the cycle life of the control group (200 cycles, CR = 28.3%).[97]

Moreover, the cycle life of batteries containing polymers formed from different structures of cyclic fluorophosphates also varies. Von Aspern *et al.* found that batteries formed from the *in situ* polymerization of PFnPrEPi monomers have lower cycle life performance compared to those formed from PFnPrEPi–CF_3.[98] This is due to the influence of the electron-withdrawing $-CF_3$ group, which leads to the formation of an effective CEI with the PFPOEPi–1CF_3 electrolyte. Analysis of the CEI thickness and composition reveals that the CEI in batteries containing PFnPrEPi thickens after cycling, with a decrease in the LiF component. In contrast, the CEI in batteries containing PFnPrEPi–CF_3 changes little after cycling, with an increase in the LiF component. These effects

are believed to contribute to the reduced cycling behavior of batteries with the PFPOEPi–1CF_3 electrolyte. Studies suggest that the introduction of larger side groups can generate lower repulsive forces or internal energy, thus limiting the occurrence of ROP and making polymerization more difficult.[99] The introduction of the side group –CF_3 in PFPOEPi–1CF_3 may reduce the degree of polymerization to some extent, leading to an increase in the number of unreacted monomers, which form a stable LiF-rich CEI on the cathode material, thereby enhancing the cycle life of the battery.

Currently, there is very limited research on the introduction of fluorinated cyclic monomers based on anionic ROP *via in situ* polymerization. However, these few examples highlight the potential of using anionic ROP to develop high-performance, fluorinated SPEs that enhance the stability and efficiency of high-energy-density batteries. By focusing on the unique reactivity of fluorinated cyclic phosphate monomers, researchers can create advanced CEI layers that protect against metal dissolution and electrolyte decomposition, ultimately improving battery longevity and performance.

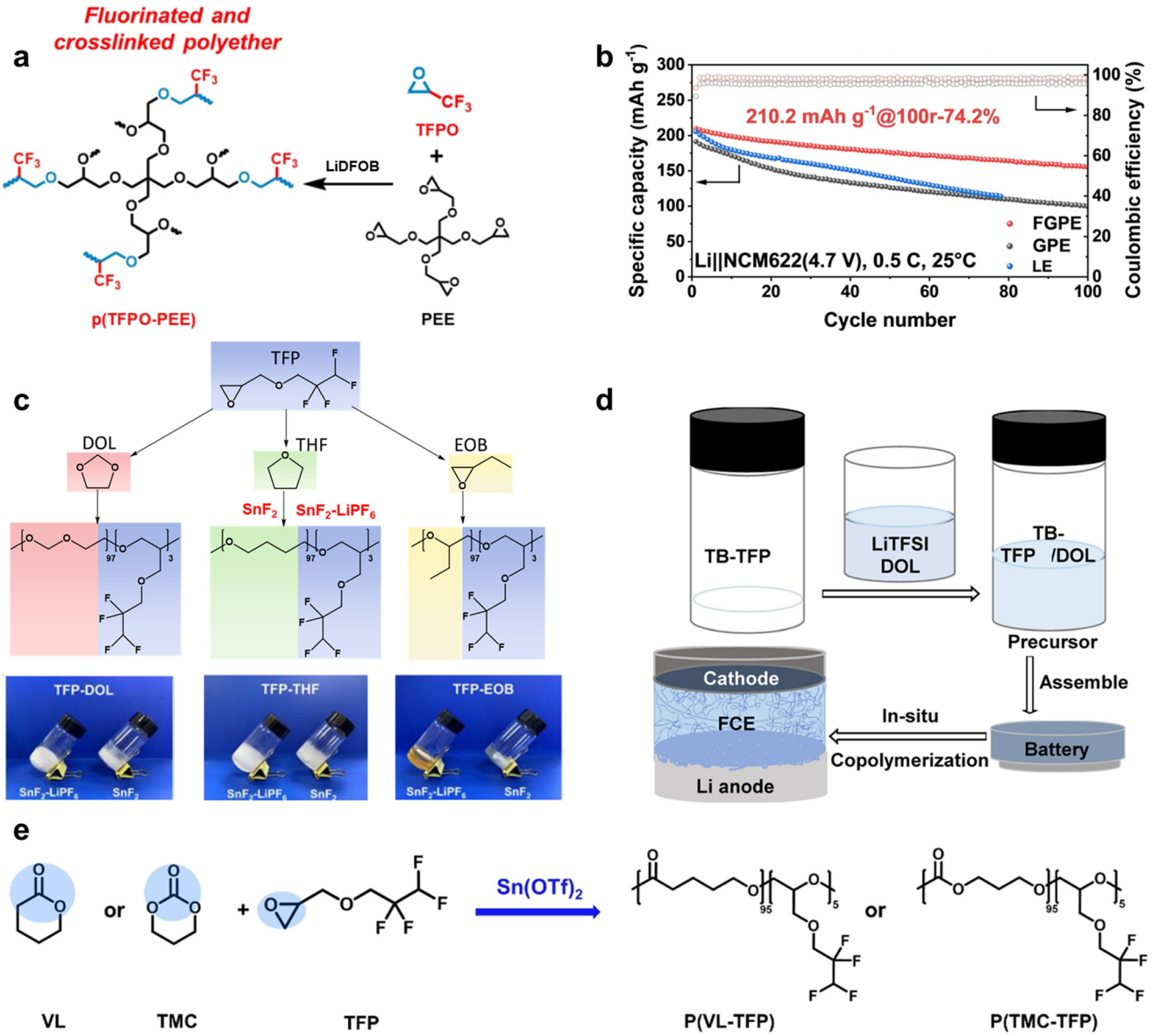

Fig. 8 Copolymerization with fluorinated monomers *via in situ* cationic ROP. (a) Synthesis routes of TFPO–PEE *via in situ* cationic ROP initiated by LiDFOB; (b) cycling performance of the Li|NCM622 battery assembled with FGPE, GPE and LE at 0.5C at a high cut-off voltage of 4.7 V. Reproduced with permission.[103] Copyright 2024, John Willey and Sons; (c) synthesis routes of TFP–DOL, TFP–THF and TFP–EOB *via in situ* cationic ROP initiated by SnF_2/SnF_2–$LiPF_6$. Reproduced with permission.[43] Copyright 2022, John Willey and Sons; (d) schematic of TFP–DOL *via in situ* cationic ROP initiated by TB in the battery. Reproduced with permission.[104] Copyright 2022, Royal Society of Chemistry; (e) the *in situ* synthesis routes for P(VL–TFP)/P(TMC–TFP) initiated by $Sn(OTf)_2$. Reproduced with permission.[105] Copyright 2023, John Wiley and Sons.

4.1.2 Cationic ROP. Cationic polymerization has garnered widespread attention from researchers because it enables the preparation of solid or quasi-solid electrolytes using traditional liquid electrolytes as monomers, without introducing impurities, and typically under mild conditions.[100] Initiators for cationic ROP fall into two main groups: protonic acids and Lewis acids. Protonic acids include sulfuric acid, trifluoroacetic acid, and fluorosulfonic acid, while Lewis acids, such as BF_3, PF_5, and $SnCl_4/SbCl_5$, and traditional lithium salts like LiDFOB and LiFSI, are commonly used for cationic ROP.[88] Most polymerization processes using these initiators do not require high temperatures. Typical monomers that can be initiated by cationic initiators include cyclic ethers, cyclic esters, cyclic acetals, cyclic amides, and more. In current reports on *in situ* polymerization for cationic ROP, the fluorination of SPEs is primarily achieved by copolymerizing fluorinated three-membered cyclic ether monomers with other cyclic ethers or cyclic esters. In this section, a classified discussion is provided based on the ring numbers of the comonomers used in the copolymerization process.

Ternary rings. The use of cationic initiators to attack the polar oxygen atoms in ethylene oxide is quite easy. However, cationic ROP is often accompanied by depolymerization and chain transfer reactions, resulting in a polymer with a broad MW distribution.[88] In contrast, the anionic ROP of ethylene oxide, characterized by its living polymerization nature, allows for effective control of MW. Despite this, cationic ROP is more reactive than anionic ROP and is therefore widely used in the fundamental research of *in situ* polymerization for SPEs.

Li *et al.* employed 1 wt% SnF_2 as an initiator to induce cationic ROP of ethylene oxide butylene oxide (EOB) with trifluoropropylene oxide (TFP). However, the resulting TFP–EOB copolymer did not cure well, forming a viscous gel after two weeks at RT (Fig. 8c).[43] When the initiator was changed to 1 wt% $LiPF_6$, cationic ROP did not occur between EOB and TFP. However, when SnF_2 and $LiPF_6$ were used together as initiators, the polymerization rate increased, and a polymer with a MW of Mw = 4.5k g mol^{-1} was formed after one week of reaction at RT. The MW of TFP–EOB is relatively low, much lower than commercially available PEO (Mw $\geq$ 100 000 g mol^{-1}). This could be due to the high ring strain in the ethylene oxide groups of EOB and TFP, leading to the initial formation of many ring-opened monomers, which hinders continuous chain growth and MW increase. Although TFP–EOB shares the same backbone structure as PEO, the lower MW of TFP–EOB results in a lower thermal degradation temperature (164 °C) compared to PEO (360 °C). The absence of significant degradation at temperatures below 90 °C suggests that only trace amounts of monomers remain in the system, which contributes to the low IC of TFP–EOB (40 °C, 0.0292 mS cm^{-1}). The study also indicates that the presence of the SnF_2–$LiPF_6$ catalyst affects the thermodynamic stability of the SPE. When SnF_2 was removed from TFP–EOB by vacuum drying, the thermal degradation temperature increased to 233 °C. Additionally, research has shown that SPEs containing the SnF_2–$LiPF_6$ catalyst exhibit poor compatibility with lithium metal,[101] but good interfacial wettability.[102] This is because SnF_2–$LiPF_6$ is a strong catalyst for both polymerization and depolymerization, and under electrochemical disturbances, rapid depolymerization may occur. This process generates a large number of monomers and oligomers, which can undergo side reactions with the lithium metal surface, compromising interfacial stability. However, since depolymerization involves a phase transition from solid to liquid, it enhances interfacial wettability, leading to a reduced overpotential in Li|Li symmetric cells.

Zhu *et al.* proposed a novel strategy for fabricating a fluorinated and crosslinked polyether-based electrolyte (FGPE) through *in situ* cationic ROP. Fluorinated monomer 3,3,3-trifluoropropene oxide (TFPO) and four-armed crosslinker PEE are initiated by the common lithium salt LiDFOB (Fig. 8a).[103] FGPE with a CCD of 4 mA cm^{-2} has good lithium metal reversibility for the reason that the Li|Li symmetrical battery assembled with it can run steadily at 0.5 mA cm^{-2} for 2000 h, which is longer than that of both non-fluorinated GPE (PDOL–PEE) and liquid electrolyte (0.68 M LiDFOB and 0.68 M LiTFSI in FEC : DMC = 1 : 1 vol%). It is observed that the Li|NCM 622 battery assembled with FGPE has excellent electrochemical stability by showing low leakage current (13.3 μA) even at 4.9 V, which guarantees it to steadily operate at 4.7 V with a CR of 74.2% after 100 cycles at 0.5C (Fig. 8b), compared to the Li|NCM 622 battery assembled with the non-fluorinated one (~50%, 100 cycles).

Quintuple rings. Quintuple rings like DOL, a prevalent ether solvent characterized by its low dielectric constant ($\varepsilon \approx 7$), can undergo polymerization at RT when catalyzed by specific cationic initiators like aluminum trifluoromethanesulfonate. This has sparked considerable research interest in recent years.[106] DOL-based SPEs offer superior flexibility, high ion conductivity, and good compatibility with lithium metal. These characteristics make DOL-based SPEs highly attractive for applications in advanced lithium-metal batteries, offering a promising combination of mechanical properties and electrochemical performance.

However, the low oxidation stability (4 V) of ether-based electrolytes remains a major challenge.[107] Cui *et al.* reported that the introduction of CF_2-groups into the middle of the ether chain of small molecule ether solvents facilitates the coordination/dissociation of Li^+ ions. This enhancement results in excellent Li-ion conductivity and heightened oxidation stability.[108] Based on previous research, Li *et al.* employed SnF_2 or SnF_2–$LiPF_6$ as a catalyst to facilitate the copolymerization of TFP with DOL and tetrahydrofuran (THF) at RT in the presence of 1.0 M LiTFSI (Fig. 8c).[43] The addition of $LiPF_6$ also accelerated the polymerization of TFP–THF and TFP–DOL, reducing the reaction time from 72 hours to 36 hours, with MWs (Mw) of 100k and 8k g mol^{-1}, respectively. Although TFP–THF and TFP–DOL have higher Mw, TFP–EOB, containing the $-O(CH_2)_2-$ backbone, exhibits

significantly higher thermal stability compared to the –O$(CH_2)_4$O– and –OCH_2O– units that constitute TFP–THF and TFP–DOL, respectively. Consequently, the thermal degradation temperatures of TFP–THF (84 °C) and TFP–DOL (76 °C) are lower. Furthermore, the IC of fluorinated TFP–DOL is 1.5–2.0 times higher than that of non-fluorinated PDOL. This enhancement in IC can be attributed to the steric hindrance imposed by the TFP units, which inhibits the self-aggregation of polymer chains.

Chen *et al.* also synthesized GPEs *via in situ* copolymerization of the fluorinated monomer TFP and DOL liquid monomer, with tris(pentafluorophenyl)borane (TB) as an initiator (Fig. 8d).[104] SEM images of the Li-metal surface in 0.03TB-TFP/9DOL reveal a mossy morphology with hardly any dead-Li observed, indicating intermediate flatness compared to liquid TFP and liquid DOL. With the introduction of fluorinated monomers, the Li|Li symmetrical battery paired with a 0.03TB-TFP/9DOL electrolyte can stably cycle for over 1600 hours at 0.1 mA cm^{-2}, while the DOL-based electrolyte alone can only cycle for 400 hours. Additionally, as the proportion of fluorinated monomers in the system increases, the monomer conversion rate of DOL during polymerization gradually decreases. This reduction is likely due to the large steric hindrance of the fluorinated end groups in TFP, which obstructs the participation of DOL in the reaction. This observation provides valuable guidance for the future design of the proportion of fluorinated monomers in such systems.

Hexagonal rings. Six-membered cyclic lactones, such as VL (valerolactone) and TMC (trimethylene carbonate), are often studied in the context of cationic ROP because their polar groups can strongly interact with lithium ions, resulting in high lithium ion solubility. The PC segments formed after the ROP of VL and TMC exhibit high electrochemical stability, making them suitable for use in high-voltage lithium battery applications. Additionally, VL and TMC monomers are relatively environmentally friendly compounds, with decomposition products that have minimal environmental impact, providing certain advantages in the development of green chemistry and sustainable battery technology.

Research indicates that the quantity of initiator used can significantly influence the electrochemical performance of electrolytes. Li *et al.* utilized $Sn(OTf)_2$ as an initiator for the cationic ROP of VL, TMC, and TFP (Fig. 8e).[105] Increasing $Sn(OTf)_2$ from 0.5 wt% to 1.5 wt% reduced the residual monomer content in P(VL–TFP) and P(TMC–TFP) from 21% to approximately 10%, alongside a decrease in IC. Despite having around 10% residual monomers, P(VL–TFP) and P(TMC–TFP) displayed low Li^+ conductivities at RT (0.02 mS cm^{-1} and 0.00035 mS cm^{-1}, respectively). The presence of residual lactone monomers notably compromised the electrochemical stability; for instance, reducing the residual VL monomer in P(VL–TFP) from 9% to 3% increased the LSV onset voltage from 3.2 V to 4.2 V, likely due to the electrochemical oxidation susceptibility of electron-rich alkoxide anions during the cationic polymerization.

Additionally, lithium salts impact monomer reaction kinetics. With 1 wt% $Sn(OTf)_2$, polymerization of P(VL–TFP) and P(TMC–TFP) at 55 °C requires five days to complete, a delay attributed to LiTFSI. Li^+ ions coordinate with VL monomers, competing with $Sn(OTf)_2$ and thereby reducing its coordination with VL and slowing the reaction.[109] Without LiTFSI, P(VL–TFP) forms a solid opaque polymer in 24 hours, while in the presence of LiTFSI, the mixture remains a viscous liquid. The molecular weight and monomer conversion rate of P(VL–TFP) without LiTFSI are notably higher compared to those with LiTFSI.

4.2. Free radical polymerization

Currently, many researchers are focusing on *in situ* construction of fluorinated copolymer electrolytes through free radical polymerization, leveraging its advantages such as flexible molecular regulation, rapid reaction kinetics, and abundant raw materials. Free radical polymerization typically begins with the initiation by free radicals, utilizing alkene monomers with unsaturated double bonds as raw materials. Polymer chains are formed by opening double bonds within the monomers and gradually linking the monomer units together.[110,111] Traditional initiators used in free radical polymerization include azo initiators, peroxy initiators, and redox initiators.[112]

In recent years, fluorinated monomers involved in *in situ* polymerization processes using radical polymerization mechanisms have been primarily fluorinated acrylic esters. These monomers copolymerize with non-fluorinated monomers. In this section, we will classify the contents based on the types of non-fluorinated comonomers. Specifically, we discuss how factors such as radical initiators and fluorinated monomers affect free radical polymerization. We will evaluate the resulting *in situ* generated SPEs in terms of electrochemical stability, cycle life, thermodynamic stability, and mechanical properties.

Acrylate system. In recent studies, Zheng *et al.* synthesized a fluorinated ASSPE, P($HFBA_{1:1}$-*co*-MEA)/LiTFSI, by incorporating 2,2,3,4,4,4-hexafluorobutyl acrylate (HFBA), 2-(2-(2-ethoxyethoxy)ethoxy)ethyl acrylate (MEA), and LiTFSI as precursors and performing *in situ* radical thermal polymerization initiated by 1 wt% BPO (Fig. 9a).[113] The MEA chains containing ether-oxide groups sustain the solvation structure of Li^+ and promote ion transportation, while the HFBA chains with electron-withdrawing fluorine groups contribute to the high electrochemical stability (LSV: 4.9 V > 4.2 V of PMEA) and lithium dissociation (t_{Li^+} = 0.36 > 0.17 of PMEA) of ASSPE. However, P(HFBA-*co*-MEA) with a rather high Mn (~12 806 g mol^{-1}) and 2.3% residual monomers might form a relatively dense chain structure, limiting the mobility of the chain segments which results in relatively low IC (0.0483 mS cm^{-1}, RT).

To enhance lithium ion transport, researchers have modified the chain segment structures of ASSPEs. Guo *et al.* synthesized three initiators for reversible addition–

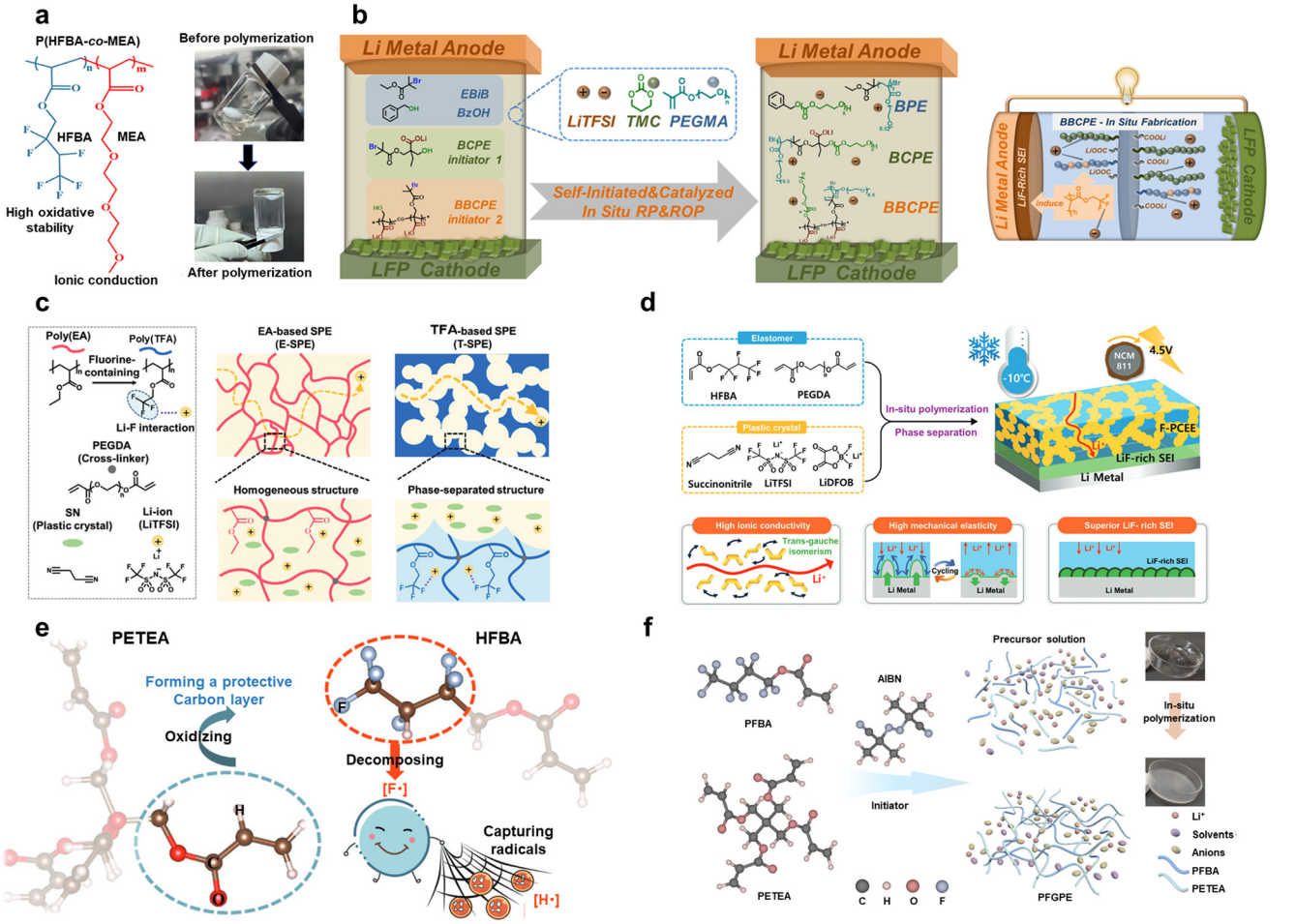

Fig. 9 Copolymerization of the acrylate system with fluorinated monomers *via* free radical polymerization. (a) Schematic of P(HFBA-*co*-MEA) before and after polymerization. Reproduced with permission.[113] Copyright 2023, American Chemical Society; (b) *in situ* fabrication of topological copolymer electrolytes *via* lithium-carboxylate-catalyzed orthogonal polymerization (left) and schematic illustration of the design concept of fluorinated BBCPE's *in situ* fabrication inside LMBs (right). Reproduced with permission.[114] Copyright 2024, American Chemical Society; (c) phase separation structure of the fluorinated GPE (T-SPE) *vs.* homogeneous structure of the non-fluorinated GPE (E-SPE). Reproduced with permission.[64] Copyright 2024, John Wiley and Sons; (d) elastomer poly(HFBA) matrix provides mechanical elasticity and facilitates the formation of a LiF-rich SEI, while the solid plastic crystal phase ensures efficient Li^+ transport through *trans–gauche* isomerism at low temperatures. Reproduced with permission.[115] Copyright 2024, John Wiley and Sons; (e) schematic diagram of synergistic flame retardant mechanisms of fluorinated GPEs. Reproduced with permission.[116] Copyright 2023, John Wiley and Sons; (f) schematic of PFGPE containing 1 M $LiPF_6$ in EC : DEC = 1 : 1 vol% before and after polymerization. Reproduced with permission.[117] Copyright 2024, Elsevier.

fragmentation chain transfer (RAFT) polymerization of poly(ethylene glycol)methyl ether (PEGMA) and ROP of TMC. This produced *in situ* polymerized blended SPEs (BPE), block-type SPEs (BCPE), and comb-type SPEs (BBCPE) (Fig. 9b).[114] BPE shows poor Li^+ transport and electrochemical stability due to Li^+ solvation mainly in PPEGMA domains and hindered diffusion in insulating PTMC domains. BCPE improves phase separation between PPEGMA and PTMC, while BBCPE achieves quasi-molecular-scale miscibility, enhancing the specific surface area of the PPEGMA/PTMC interface. This promotes effective Li^+ coordination with ether/carbonate units (IC = 0.25 mS cm^{-1} at 30 °C, t_{Li^+} = 0.51 at 60 °C) and combines the advantages of PPEGMA and PTMC segments. With the addition of TFMA, the Li|LFP battery assembled with BBCPE exhibited stable long cycling performance even at high rates, retaining more than 76% of its capacity after 1000 cycles at 2C and above 73% after 1000 cycles at 3C.

To enhance the IC of SPEs, researchers typically synthesize GPEs by incorporating fluorinated polymer matrices with solvents as well. SN combined with a LiTFSI solution is commonly chosen as the solvent due to its ability to achieve high bulk IC (~1 mS cm^{-1} at RT) and excellent oxidation stability. Recently, 2,2,2-trifluoroethyl acrylate (TFA),[64,82] 2,2,3,4,4,4-hexafluorobutyl methacrylate (HFBMA),[65] and HFBA,[115] combined with crosslinkers like poly(ethylene glycol)diacrylate (PEGDA), have been reported to construct fluorinated polymer matrices in SN-LiTFSI solution. Han *et al.* used TFA and EA as monomers, AIBN as an initiator, PEGDA as a crosslinker, and SN-LiTFSI as a solvent to synthesize an *in situ* fluorinated GPE (T-SPE) and non-fluorinated GPE (E-SPE). It turns out that the fluorine atoms

in the fluoropolymer matrix enhanced its hydrophobicity, facilitating phase separation from the SN-LiTFSI solution. In contrast, the E-SPE exhibited a homogeneous structure (Fig. 9c).[64] This bi-continuous structure of F-containing elastomers and SN plastic crystals not only enhances the mechanical strength of GPEs but also creates robust LiF-rich interphases, enabling excellent stability to match high voltage batteries. The Li|NCM battery assembled with the T-SPE has a better CR after 100 cycles at 1 mA cm^{-2} compared with that with the E-SPE. The full battery (RT), with 5 μm Li-metal, high-loading (>11 mg cm^{-2}) NCM-83, low $N/P < 0.5$, and a high-operating voltage of 4.5 V, has achieved a high energy density of 393 W h kg^{-1}.

The researchers also explored the low-temperature operating performance of this fluorinated GPE containing SN-LiTFSI. Park *et al.* used HFBA and BA as monomers, AIBN as an initiator, PEGDA as a crosslinker, and SN-LiTFSI as a solvent to synthesize an *in situ* fluorinated GPE (H-SPE) and non-fluorinated GPE (B-SPE) (Fig. 9d).[115] The H-SPE, due to the high fluorine content in the elastic phase, exhibits weak interactions with Li^+, leading to an increased lithium ion concentration in the plastic crystalline phase, which facilitates SN transport (IC ≈ 0.23 mS cm^{-1} of H-SPE > 0.003 mS cm^{-1} of B-SPE at −10 °C). In addition, the high-mechanical-elasticity H-SPE can accommodate significant volume changes and suppress lithium dendrite growth, ensuring stable contact with the lithium metal anode throughout discharge. In contrast, B-SPEs suffer from permanent deformation during charging, resulting in loss of contact between the electrolyte and the electrode after discharge due to their limited mechanical elasticity. Therefore, the cycling performance of Li|NCM811 assembled with the H-SPE (150 cycles, 85.3%) is better than the one with the B-SPE at a cut-off voltage of 4.5 V operated at −10 °C.

Although the F-containing phase-separation SPE system holds significant promise for achieving high-energy LMBs and is suitable for future practical battery applications, the confirmation of the degree of fluorination remains to be discussed. Qin *et al.* used TFA and 2-(2-ethoxyethoxy)ethyl acrylate as monomers and AIBN as an initiator to construct a polymer matrix in the SN-LiTFSI solution.[82] According to the linear sweep voltammetry (LSV) results: for the non-fluorinated electrolyte (4.7 V), fully fluorinated electrolyte (4.25 V), and partially fluorinated electrolyte (5.0 V), it appears that a high degree of fluorination might lead to insufficient polymerization, and the residual monomers might participate in the high voltage oxidation reaction. Therefore, the residual unpolymerized monomer would decrease the ESW of SPEs.

Conventional liquid solvents have also been used in fluorinated GPEs owing to their advantageous properties such as excellent solubility with lithium salts, low viscosity, low toxicity, and relatively low cost. However, they are accompanied by decreased thermal stability due to the flammability of carbonate solvents. During combustion, electrolytes produce flammable vapors, such as gaseous carbonate or ether solvent (RH), when exposed to high temperatures. Subsequently, these vapors decompose to yield H· radicals (RH → R· + H·), which then react with oxygen from the cathode to generate HO· radicals (H· + O_2 → HO· + O·). These free radicals engage in a chain of reactions with hydrogen, leading to combustion (HO· + H_2 → H· + H_2O; O· + H_2 → HO· + H·).[118] To overcome this issue, researchers introduce fluorinated monomers known for high thermal stability and non-flammability, such as perfluorobutyl acrylate (PFBA),[117] TFPMA,[83] 3,3,4,4,5,5,6,6,7,7,8,8-tridecafluorooctyl acrylate,[119] and HFBA,[120] into polymer matrices. Hu *et al.* proposed a synergistic flame retardant mechanism of fluorinated GPEs (Fig. 9e), They discovered that the I_D/I_G value in the Raman spectra of PETEA is lower than that of PETEA–HFBA, indicating that PETEA chains in the polymer form a more stable graphitized carbon layer after combustion. This protective layer blocks oxygen and heat required for combustion, while F· radicals decomposed by HFBA chains effectively inhibit the chain combustion reaction of H· radicals. Yang *et al. in situ* synthesized a fluorinated GPE (PFGPE) with PFBA and PETEA (Fig. 9f) and found that PFGPE is flame retardant when continuously exposed to fire. On the other hand, the liquid carbonate electrolyte burns easily and produces considerable heat. Xu *et al.* synthesized an FP crosslinker for LMBs by introducing fluoroalkyl into the phosphate crosslinker, significantly improving the fire-retardant effectiveness of FP-GPE and ensuring heightened safety standards for high-voltage LMBs. FP-GPE exhibited excellent safety without electrolyte leakage or combustion compared to the liquid electrolyte after being penetrated by a metal nail. Moreover, the incorporation of fluorinated segments endows FP-GPE with high electrochemical stability toward high-voltage cathode materials, as confirmed by electrochemical floating analysis showing no remarkable oxidation in FP-GPE below 4.9 V (*vs.* Li/Li^+).[121] Zhou *et al.* used TFMA and PETEA to construct a polymer matrix (AFPE10) containing FEC. A Li-LCO battery assembled with AFPE10 achieved 507 W h kg^{-1}, operating for 200 cycles with a CR of 80%. Abuse tests on the pouch cell assembled with AFPE10 demonstrated its exceptional safety, as the light bulb on the pouch cell kept operating even when bent, cut open, or exposed to flame.

Vinylidene carbonate (VC) system. Vinylidene Carbonate (VC) and Vinyl Ethylene Carbonate (VEC) have been employed as monomers in the development of ASSPEs due to their high dielectric constants and excellent lithium salt solubility. Li *et al.* explored the copolymerization of VC and VEC with the fluorinated monomer TFPMA using AIBN as the initiator (Fig. 10a).[105] At 80 °C for 18 hours, a reddish-brown SPE was obtained. Increasing the AIBN concentration from 0.5 wt% to 1.5 wt% reduced residual VEC from 56% to 45%, with a corresponding decrease in IC. VC, under similar conditions, produced an opaque, rigid solid with low IC (0.02 mS cm^{-1}) due to cross-linking from radical transfer during P(VC–TFPMA) polymerization, which diminishes flexibility.[122] In contrast, P(VEC–TFPMA) polymerized more slowly with 1

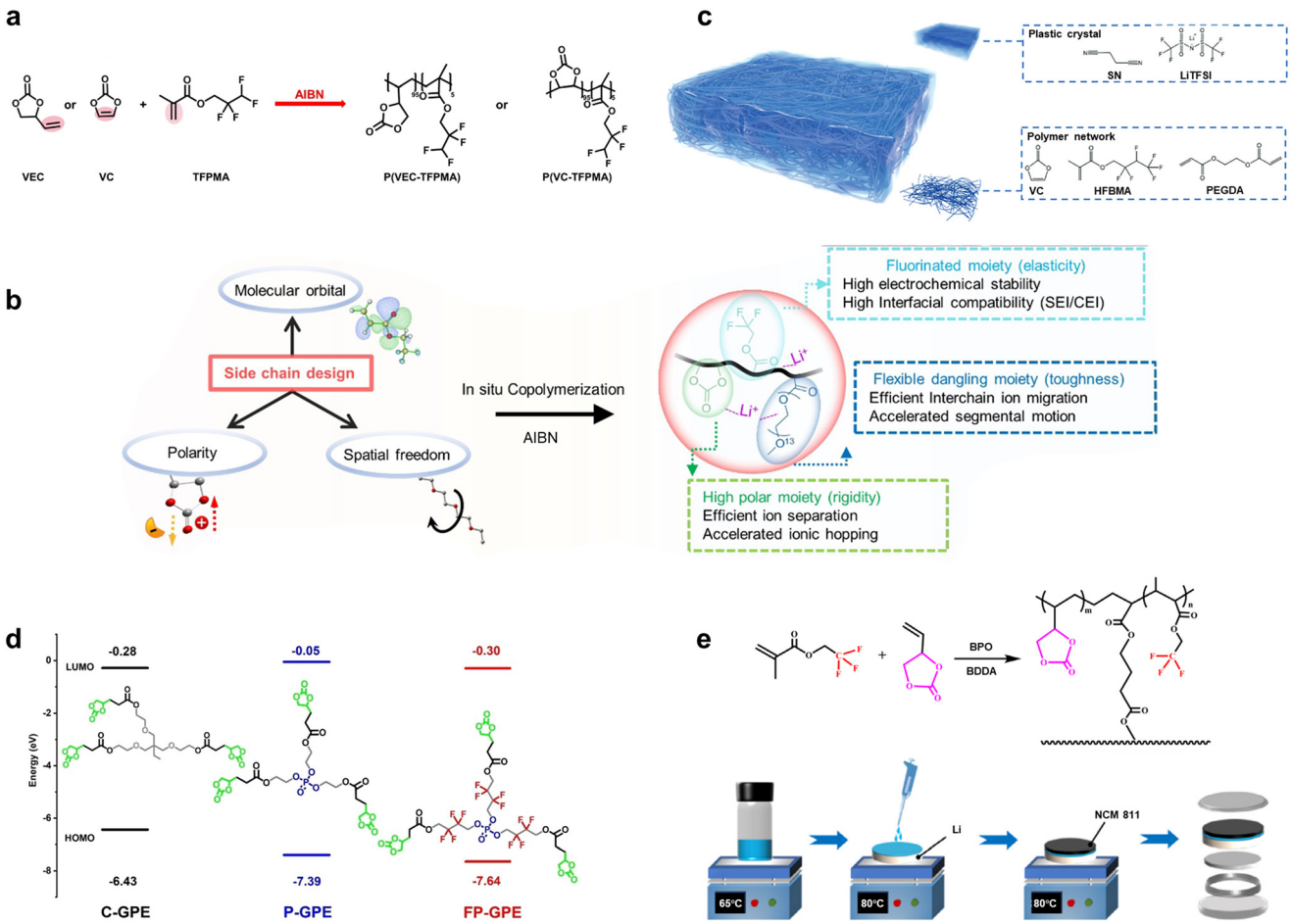

Fig. 10 Copolymerization of the VC system and fluorinated monomers *via* free radical polymerization. (a) The synthesis routes for P(VEC–TFPMA)/P(VC–TFPMA). Reproduced with permission.[105] Copyright 2023, John Wiley and Sons; (b) side chain design strategy for the ternary copolymer SPE. Reproduced with permission.[124] Copyright 2024, John Wiley and Sons; (c) schematic diagram of P(VC-*co*-HFBMA) containing SN-LiTFSI. Reproduced with permission.[65] Copyright 2024, John Wiley and Sons; (d) the HOMO and LUMO energy levels of ETPTA, TAEP and FP cross-linker. Reproduced with permission.[121] Copyright 2024, John Wiley and Sons; (e) schematic of the *in situ* polymerization technology for the coin cell assembled with P(VEC-*co*-TFMA). Reproduced with permission.[125] Copyright 2022, Elsevier.

wt% AIBN, requiring 30 hours to complete and achieving an IC of 0.2 mS cm^{-1} at RT, indicating better stability. Additionally, the presence of lithium salts accelerates VEC polymerization and improves monomer conversion rates.[123]

Xu *et al.* utilized 0.5 wt% AIBN to initiate the free radical copolymerization of TFA, VC, and PEGMEA, resulting in a ternary copolymer CPE (Fig. 10b).[124] Monomer conversion rates were 99% for PTFEA, 82% for PVC, and 83.3% for CPE. The electron-withdrawing oxygen atoms in VC reduce its electron cloud density, whereas TFA's high electron density accelerates polymerization. The high lithium-ion conductivity of CPE (2.19 mS cm^{-1}, t_{Li^+} = 0.59 at 30 °C) is due to PVC enhancing lithium salt dissociation and increasing free carrier concentration, while PEGMEA improves polymer chain mobility for long-range ion transfer. Residual VC coordinates with lithium ions, further boosting IC through a vehicle transport mechanism. The inclusion of fluorinated monomers in CPE ensures high lithium metal reversibility, strong electrochemical stability, and extended cycle life. CPE maintains stable cycling for 1000 hours at 0.8 mA cm^{-2} in the Li|Li symmetric battery and shows stable performance (200 cycles, CR = 90%) at cut-off *v* (4.3 V) and 0.5C in the Li|NCM811 battery.

Peng *et al.* employed 0.5 wt% AIBN and 1 mol% PEGDA to *in situ* polymerize VC and HFBMA at 60 °C, forming a polymer matrix with the SN-LiTFSI deep eutectic solvent embedded, resulting in the PFV electrolyte (Fig. 10c). DFT analysis shows HFBMA's lower LUMO (−0.40 eV) compared to VC (0.98 eV), indicating HFBMA's higher reactivity and faster polymerization rate. The SPE, with 32% residual VC monomers or oligomers, combined with SN solvent molecules, enhances lithium ion transport (IC = 0.63 mS cm^{-1}, t_{Li^+} = 0.82). The polymer's Mw of 38 640 g mol^{-1} confirms successful cross-linking, improving both mechanical properties and IC. The fluorinated polymer matrix and SN stabilize the electrolyte under high cut-off voltage, enhancing electrochemical stability (LSV = 5.1 V). Additionally, the Li|NCM811 cell with PFV exhibits a specific

capacity of 193.2 mA h g^{-1} and 81.5% CR after 100 cycles, outperforming the non-fluorinated PV (64.5%) in CR.

Xu *et al.* synthesized an FP cross-linker containing an abundant fluorine reservoir.[121] They used 0.19 wt% ABVN as the initiator and 5.65 wt% of ETPTA/TAEP/FP monomers as cross-linking agents. The monomer VC was *in situ* polymerized with each of the three cross-linking agents at 60 °C to form polymer matrices. 1 M $LiPF_6$ in EC (1 : 1 vol%) electrolyte was embedded within the polymer matrices, resulting in three types of SPEs: C-GPE, P-GPE, and FP-GPE (Fig. 10d). FP-GPE exhibited a lower LUMO level than P-GPE (−0.30 eV for FP-GPE, compared to −0.05 eV for P-GPE), suggesting that FP-GPE more readily decomposes on the surface of lithium metal to produce a LiF-rich SEI. FP-GPE displayed a smaller overpotential and operated for over 700 hours in a Li|Li symmetrical battery, demonstrating higher stability and compatibility with lithium metal. In contrast, a Li|Li symmetrical battery assembled with P-GPE ran for only about 150 hours with a larger overpotential, indicating higher reactivity between lithium metal and non-fluorinated P-GPE.

Wang *et al.* used 0.3 wt% BPO as the initiator and 3 wt% BDDA as the cross-linker to *in situ* polymerize VEC and TFMA at 65 °C, producing P(VEC-*co*-TFMA) (Fig. 10e).[125] With LiTFSI at 40 wt%, increasing the TFMA content (up to 30 wt%) enhances VEC polymerization activity due to the fluorine atoms, resulting in a gradual increase in Mw. However, when TFMA content exceeds 30 wt%, the steric hindrance of fluorinated segments inhibits further reaction, decreasing Mw. The Mw peaks at 30 wt% TFMA (25.08 kg mol^{-1}), three times that of the homopolymer PVEC, improve the mechanical properties of the SPE. Besides, fluorinated monomers increase lithium salt dissociation, but excessive TFMA (>30 wt%) creates strong internal interactions that reduce IC by impeding Li^+ transport. The optimal composition, FPCSPE 3–40 (30 wt% TFMA + 40 wt% LiTFSI), achieves a specific capacity of 218 mA h g^{-1} and 70% CR over 300 cycles at RT and 4.5 V in Li|NCM811 cells.

5. Summary and outlook

Overall, *in situ* polymerization offers excellent interface compatibility and is highly compatible with industrial battery production lines. Fluorinated polymer electrolytes can generate LiF-rich SEIs and CEIs, which is beneficial for forming dendrite-free interfaces between electrodes and SPEs, thereby providing batteries with opportunities to achieve long cycling lifespan. Additionally, the strong electrochemical stability of C–F ensures compatibility with high-voltage cathode materials and excellent thermal stability. In conclusion, currently, *in situ* polymerization of fluorinated SPEs has great potential for designing high-voltage and long-cycling LMBs, as summarized in Table 1.

However, there are still some challenges to overcome before practical applications can be realized. Fabricating SPEs *via in situ* polymerization while considering the characteristics of fluorination is a multidisciplinary endeavor. The future of energy storage, based on *in situ* polymerization for fluorinated SPEs, is fraught with challenges, mainly as follows:

(1) Selection of fluorine-containing monomers. Currently, fluoroacrylates such as TFA, TFMA, HFBA, HFBMA, and PFBA are used to synthesize SPEs *via* free radical polymerization, while fluorinated propylene oxides such as TFP and TFPO are employed for ionic polymerization. The presence of terminal fluorine atoms in monomers significantly influences the entire polymerization process. Both the concentration of fluorinated monomers in the precursor solution and the number of fluorine atoms within the monomer itself profoundly affect the degree of polymerization of SPEs. This can potentially result in incomplete polymerization, leading to residual monomers that may decrease the electrochemical window of the SPEs, thereby impacting the high-voltage stability of batteries. Therefore, it is urgent to develop new monomers different from traditional fluorinated monomers that can act as both polymerization monomers and effective

Table 1 Summary of performances of current *in situ* polymerized fluorinated polymer electrolytes

SPE	σ at RT (mS cm^{-1})	LSV (V)	NCM cut-off U (V)	Loading (mg cm^{-2})	Capacity retention	Ref.
PEE–TFPO + 75% FEC/DMC (1 : 1 vol%) + 12% LiTFSI + 6% LiDFOB[a]	3.98	5.10	4.70	8.70	74.2% (100 cycles, 0.5C)	103
TFP + 65% VL + 28% LiTFSI[a]	0.02	3.20	4.40	2.50	48.9% (100 cycles, 0.2C)	105
TFPMA + 65% VEC + 28% LiTFSI[b]	0.20	>4.20	4.40	2.50	89.7% (100 cycles, 0.2C)	105
TFMA–BDDA + 30% VEC + 40% LiTFSI[b]	0.05	~5.20	4.50	1.30	70.0% (300 cycles, 0.1C)	125
PFBA–PETEA + 97% electrolyte (1 M $LiPF_6$ in EC : DEC = 1 : 1 vol%)[b]	0.56	5.00	4.40	~30.50	83.4% (120 cycles, 0.2C charge, 0.5C discharge)	117
HFBMA–PEGDA–36% VC + 22% SN + 6% LiTFSI[b]	0.63	5.10	4.30	2.50	81.5% (100 cycles, 0.5C)	65
TFA–PEGDA + 42% SN + 5% FEC 11% LiTFSI + 1.3% LiDFOB[b]	0.90	—	4.30	>11.00	~70.0% (100 cycles, 0.5C)	64
FP–19% VC + 75% electrolyte (1 M $LiPF_6$ in FEC : FEMC = 3 : 7 vol% with 2% $LiBF_4$)[b]	4.45	—	4.30	20.84	85.2% (100 cycles, 0.3C)	121
HFBA–40% MEA + 23% LiTFSI[b]	0.0483	4.90	4.30	0.96	62.3% (700 cycles, 0.1C)	113
EA–14% EDA + 45% SN + 27% LiTFSI[b]	0.70	4.90	4.30	11.53	93.3% (60 cycles, 0.2C)	126

[a] Ionic polymerization. [b] Free radical polymerization.

SEI/CEI-forming additives simultaneously, addressing the issue of residual unpolymerized monomers.

(2) Selection of fluorinated additives. Current research on *in situ* polymerization of SPEs primarily focuses on film-forming FEC additives. Concerning sacrificial additives, the presence of strong C–F bonds makes them highly stable, posing challenges in activating these bonds to promote the formation of more LiF species. Furthermore, reducing the detachment of the SEI/CEI with poor lithium affinity from the anode/cathode respectively remains to be addressed. The development of novel and efficient fluorinated additives to facilitate the uniform and rapid formation of a lithium-conductive SEI/CEI on both electrodes continues to be a challenge. Here, we propose utilizing computational simulations to design molecular structures and subsequently validating the feasibility of these designs through experimentation as a promising avenue.

(3) Optimization of initiation conditions. The dosage of initiators has a certain impact on the amounts of residual monomers. Typically, a decreased dosage of initiators tends to increase the residual monomers after polymerization, which may enhance the ion conductivity of batteries but diminish the ESW. Residual fluorinated monomers after polymerization may result in the formation of excessively thick SEI/CEI layers, impeding the migration of Li^+. Furthermore, temperature and time during polymerization should also be strictly controlled. For instance, in free radical polymerization, the electron-rich group –CN in AIBN may react with metallic lithium, deteriorating battery performance. Excessive polymerization temperature may promote reactions between –CN and electrode materials. Thus, selecting appropriate polymerization temperature and time is imperative.

(4) Consideration of mechanical properties. While *in situ* polymerization techniques can establish good interface compatibility before battery cycling, the lithium expansion effect during cycling may lead to phenomena such as loss of contact in the battery. Therefore, this necessitates SPEs with higher mechanical and elastic properties to suppress dendrite growth and penetration. However, some fluorinated GPEs typically incorporate a significant amount of electrolyte (>40%) to achieve high ion conductivity, lacking characterization related to mechanical properties.

(5) Importance of supported membranes. Supported membranes are crucial in the *in situ* polymerization preparation process as they prevent short circuits between the positive and negative electrodes before polymerization. In the precursor solution of fluorinated SPEs, due to the presence of a large amount of polar fluorinated monomers/additives, the wettability of the membrane may be poor, significantly affecting battery performance. Additionally, the mechanical properties, chemical stability, and thermal stability of the membrane should also be comprehensively considered for future industrial production.

(6) Environmental influence of fluorinated SPEs. Fluorinated SPEs offer superior battery performance due to their high chemical stability, which also means poor biodegradability. The strong C–F bonds in these polymers resist degradation by microorganisms or environmental factors, leading to their long-term persistence in the environment. Accumulation of fluorinated materials can be toxic to aquatic life and wildlife. Traditional waste management methods, such as landfilling or incineration, are ineffective for these materials and may cause secondary pollution. High-temperature conditions can release toxic fluorinated gases, posing risks to health and the environment. To address these issues, researchers should explore non-fluorinated alternatives with better environmental compatibility and improve recycling processes for existing fluorinated polymers to reduce toxicity. However, research on non-fluorinated alternatives is still in its early stages, and they are primarily studied in conjunction with traditional fluorinated electrolytes as effective co-components. Developing degradable fluorinated SPEs and using green chemistry to minimize harmful by-products are also promising approaches. Balancing technical performance with environmental impact will be crucial in future developments.

Data availability

No primary research results, software or code have been included and no new data were generated or analyzed as part of this review.

Conflicts of interest

The authors declare no conflict of interest.

Acknowledgements

This work is supported by the National Natural Science Foundation of China (22022813), the Zhejiang Provincial Natural Science Foundation of China (LQ24B030002), and the China Postdoctoral Science Foundation (2022M722729, 2023T160571).

References

1 K. Qin, K. Holguin, M. Mohammadiroudbari, J. Huang, E. Y. S. Kim, R. Hall and C. Luo, Strategies in structure and electrolyte design for high-performance lithium metal batteries, *Adv. Funct. Mater.*, 2021, **31**, 2009694.
2 G. M. Hobold, J. Lopez, R. Guo, N. Minafra, A. Banerjee, Y. Shirley Meng, Y. Shao-Horn and B. M. Gallant, Moving beyond 99.9% Coulombic efficiency for lithium anodes in liquid electrolytes, *Nat. Energy*, 2021, **6**, 951–960.
3 D. Lin, Y. Liu and Y. Cui, Reviving the lithium metal anode for high-energy batteries, *Nat. Nanotechnol.*, 2017, **12**, 194–206.
4 L. Sun, K. Higaki and R. C. McDonald, Performance characteristics of lithium-ion cells using in-situ polymerized electrolytes, *J. Power Sources*, 1997, **68**, 352–356.

5 Q. Liu, L. Wang and X. He, Toward practical solid-state polymer lithium batteries by in-situ polymerization process: A review, *Adv. Energy Mater.*, 2023, **13**, 2300798.
6 W. Huang, T. Liu, L. Yu, J. Wang, T. Zhou, J. Liu, T. Li, R. Amine, X. Xiao, M. Ge, L. Ma, S. N. Ehrlich, M. V. Holt, J. Wen and K. Amine, Unrecoverable lattice rotation governs structural degradation of single-crystalline cathodes, *Science*, 2024, **384**, 912–919.
7 S. Huo, L. Sheng, W. Xue, L. Wang, H. Xu, H. Zhang and X. He, Challenges of polymer electrolyte with wide electrochemical window for high energy solid-state lithium batteries, *InfoMat*, 2023, **5**, e12394.
8 X. Yang, M. Jiang, X. Gao, D. Bao, Q. Sun, N. Holmes, H. Duan, S. Mukherjee, K. Adair, C. Zhao, J. Liang, W. Li, J. Li, Y. Liu, H. Huang, L. Zhang, S. Lu, Q. Lu, R. Li, C. V. Singh and X. Sun, Determining the limiting factor of the electrochemical stability window for PEO-based solid polymer electrolytes: Main chain or terminal –OH group?, *Energy Environ. Sci.*, 2020, **13**, 1318–1325.
9 H. Wang, L. Sheng, G. Yasin, L. Wang, H. Xu and X. He, Reviewing the current status and development of polymer electrolytes for solid-state lithium batteries, *Energy Storage Mater.*, 2020, **33**, 188–215.
10 Q. Huang, J. Song, Y. Gao, D. Wang, S. Liu, S. Peng, C. Usher, A. Goliaszewski and D. Wang, Supremely elastic gel polymer electrolyte enables a reliable electrode structure for silicon-based anodes, *Nat. Commun.*, 2019, **10**, 5586.
11 L. Tang, B. Chen, Z. Zhang, C. Ma, J. Chen, Y. Huang, F. Zhang, Q. Dong, G. Xue, D. Chen, C. Hu, S. Li, Z. Liu, Y. Shen, Q. Chen and L. Chen, Polyfluorinated crosslinker-based solid polymer electrolytes for long-cycling 4.5 V lithium metal batteries, *Nat. Commun.*, 2023, **14**, 2301.
12 Z. Li, Y. Chen, X. Yun, P. Gao, C. Zheng and P. Xiao, Critical review of fluorinated electrolytes for high-performance lithium metal batteries, *Adv. Funct. Mater.*, 2023, **33**, 2300502.
13 Y. Wang, Z. Li, Y. Hou, Z. Hao, Q. Zhang, Y. Ni, Y. Lu, Z. Yan, K. Zhang, Q. Zhao, F. Li and J. Chen, Emerging electrolytes with fluorinated solvents for rechargeable lithium-based batteries, *Chem. Soc. Rev.*, 2023, **52**, 2713–2763.
14 Y. Su, X. Rong, A. Gao, Y. Liu, J. Li, M. Mao, X. Qi, G. Chai, Q. Zhang, L. Suo, L. Gu, H. Li, X. Huang, L. Chen, B. Liu and Y.-S. Hu, Rational design of a topological polymeric solid electrolyte for high-performance all-solid-state alkali metal batteries, *Nat. Commun.*, 2022, **13**, 4181.
15 X. Wang, C. Zhang, M. Sawczyk, J. Sun, Q. Yuan, F. Chen, T. C. Mendes, P. C. Howlett, C. Fu, Y. Wang, X. Tan, D. J. Searles, P. Král, C. J. Hawker, A. K. Whittaker and M. Forsyth, Ultra-stable all-solid-state sodium metal batteries enabled by perfluoropolyether-based electrolytes, *Nat. Mater.*, 2022, **21**, 1057–1065.
16 D. H. C. Wong, J. L. Thelen, Y. Fu, D. Devaux, A. A. Pandya, V. S. Battaglia, N. P. Balsara and J. M. DeSimone, Nonflammable perfluoropolyether-based electrolytes for lithium batteries, *Proc. Natl. Acad. Sci. U. S. A.*, 2014, **111**, 3327–3331.
17 Q. Zhou, J. Ma, S. Dong, X. Li and G. Cui, Intermolecular chemistry in solid polymer electrolytes for high-energy-density lithium batteries, *Adv. Mater.*, 2019, **31**, 1902029.
18 Z. Li, R. Yu, S. Weng, Q. Zhang, X. Wang and X. Guo, Tailoring polymer electrolyte ionic conductivity for production of low- temperature operating quasi-all-solid-state lithium metal batteries, *Nat. Commun.*, 2023, **14**, 482.
19 J. Li, H. Hu, W. Fang, J. Ding, D. Yuan, S. Luo, H. Zhang and X. Ji, Impact of fluorine-based lithium salts on SEI for all-solid-state PEO-based lithium metal batteries, *Adv. Funct. Mater.*, 2023, **33**, 2303718.
20 Y. Yamada, J. Wang, S. Ko, E. Watanabe and A. Yamada, Advances and issues in developing salt-concentrated battery electrolytes, *Nat. Energy*, 2019, **4**, 269–280.
21 X. Zhang, M. Zhang, J. Wu, X. Hu, B. Fu, Z. Zhang, B. Luo, K. Khan, Z. Fang, Z. Xu and M. Wu, Lewis acid fluorine-donating additive enables an excellent semi-solid-state electrolyte for ultra-stable lithium metal batteries, *Nano Energy*, 2023, **115**, 108700.
22 M. Ma, F. Shao, P. Wen, K. Chen, J. Li, Y. Zhou, Y. Liu, M. Jia, M. Chen and X. Lin, Designing weakly solvating solid main-chain fluoropolymer electrolytes: Synergistically enhancing stability toward Li anodes and high-voltage cathodes, *ACS Energy Lett.*, 2021, **6**, 4255–4264.
23 J. Christensen and J. Newman, A mathematical model for the lithium-ion negative electrode solid electrolyte interphase, *J. Electrochem. Soc.*, 2004, **151**, A1977.
24 D. Aurbach, Review of selected electrode–solution interactions which determine the performance of Li and Li ion batteries, *J. Power Sources*, 2000, **89**, 206–218.
25 E. Peled, D. Golodnitsky and G. Ardel, Advanced model for solid electrolyte interphase electrodes in liquid and polymer electrolytes, *J. Electrochem. Soc.*, 1997, **144**, L208–L210.
26 Y. Li, Y. Li, A. Pei, K. Yan, Y. Sun, C.-L. Wu, L.-M. Joubert, R. Chin, A. L. Koh, Y. Yu, J. Perrino, B. Butz, S. Chu and Y. Cui, Atomic structure of sensitive battery materials and interfaces revealed by cryo–electron microscopy, *Science*, 2017, **358**, 506–510.
27 J. Tan, J. Matz, P. Dong, J. Shen and M. Ye, A growing appreciation for the role of LiF in the solid electrolyte interphase, *Adv. Energy Mater.*, 2021, **11**, 2100046.
28 W. Li, G. Wu, C. M. Araújo, R. H. Scheicher, A. Blomqvist, R. Ahuja, Z. Xiong, Y. Feng and P. Chen, Li^+ ion conductivity and diffusion mechanism in α-Li_3N and β-Li_3N, *Energy Environ. Sci.*, 2010, **3**, 1524.
29 Y. C. Chen, C. Y. Ouyang, L. J. Song and Z. L. Sun, Electrical and lithium ion dynamics in three main components of solid electrolyte interphase from density functional theory study, *J. Phys. Chem. C*, 2011, **115**, 7044–7049.
30 W. D. Richards, L. J. Miara, Y. Wang, J. C. Kim and G. Ceder, Interface stability in solid-state batteries, *Chem. Mater.*, 2016, **28**, 266–273.

31 A. Budi, A. Basile, G. Opletal, A. F. Hollenkamp, A. S. Best, R. J. Rees, A. I. Bhatt, A. P. O'Mullane and S. P. Russo, Study of the initial stage of solid electrolyte interphase formation upon chemical reaction of lithium metal and N -methyl- N -propyl-pyrrolidinium-bis(fluorosulfonyl)imide, *J. Phys. Chem. C*, 2012, **116**, 19789–19797.

32 J. Wang, Y. Yamada, K. Sodeyama, C. H. Chiang, Y. Tateyama and A. Yamada, Superconcentrated electrolytes for a high-voltage lithium-ion battery, *Nat. Commun.*, 2016, **7**, 12032.

33 J. Zheng, S. Chen, W. Zhao, J. Song, M. H. Engelhard and J.-G. Zhang, Extremely Stable sodium metal batteries enabled by localized high-concentration electrolytes, *ACS Energy Lett.*, 2018, **3**, 315–321.

34 A. Wang, S. Geng, Z. Zhao, Z. Hu and J. Luo, In-situ cross-linked plastic crystal electrolytes for wide-temperature and high-energy-density lithium metal batteries, *Adv. Funct. Mater.*, 2022, **32**, 2201861.

35 W. Zhang, V. Koverga, S. Liu, J. Zhou, J. Wang, P. Bai, S. Tan, N. K. Dandu, Z. Wang, F. Chen, J. Xia, H. Wan, X. Zhang, H. Yang, B. L. Lucht, A.-M. Li, X.-Q. Yang, E. Hu, S. R. Raghavan, A. T. Ngo and C. Wang, Single-phase local-high-concentration solid polymer electrolytes for lithium-metal batteries, *Nat. Energy*, 2024, **9**, 386–400.

36 Y. Wang, X. Yang, Y. Meng, Z. Wen, R. Han, X. Hu, B. Sun, F. Kang, B. Li, D. Zhou, C. Wang and G. Wang, Fluorine chemistry in rechargeable batteries: Challenges, progress, and perspectives, *Chem. Rev.*, 2024, **124**, 3494–3589.

37 S.-J. Park, J.-Y. Hwang, C. S. Yoon, H.-G. Jung and Y.-K. Sun, Stabilization of lithium-metal batteries based on the in-situ formation of a stable solid electrolyte interphase layer, *ACS Appl. Mater. Interfaces*, 2018, **10**, 17985–17993.

38 T. Li, X.-Q. Zhang, P. Shi and Q. Zhang, Fluorinated solid-electrolyte interphase in high-voltage lithium metal batteries, *Joule*, 2019, **3**, 2647–2661.

39 A. L. Michan, B. S. Parimalam, M. Leskes, R. N. Kerber, T. Yoon, C. P. Grey and B. L. Lucht, Fluoroethylene carbonate and vinylene carbonate reduction: Understanding lithium-ion battery electrolyte additives and solid electrolyte interphase formation, *Chem. Mater.*, 2016, **28**, 8149–8159.

40 J. Zhu, J. Zhang, R. Zhao, Y. Zhao, J. Liu, N. Xu, X. Wan, C. Li, Y. Ma, H. Zhang and Y. Chen, In-situ 3D crosslinked gel polymer electrolyte for ultra-long cycling, high-voltage, and high-safety lithium metal batteries, *Energy Storage Mater.*, 2023, **57**, 92–101.

41 J. Xie, S. Y. Sun, X. Chen, L. P. Hou, B. Q. Li, H. J. Peng, J. Q. Huang, X. Q. Zhang and Q. Zhang, Fluorinating the solid electrolyte interphase by rational molecular design for practical lithium-metal batteries, *Angew. Chem., Int. Ed.*, 2022, **61**, e202204776.

42 A. Wang, Y. Nie, Y. Zhao, D. Xu, L. Zhang, Z. Zhao, L. Ren, S. Zhou, X. Liu and J. Luo, Functional copolymer derived self-adapting LiF-rich interphase toward deep cycling lithium metal batteries, *Adv. Funct. Mater.*, 2024, 2401462.

43 W. Li, L. Ma, S. Liu, X. Li, J. Gao, S. m. Hao and W. Zhou, Thermally depolymerizable polyether electrolytes for convenient and low-cost recycling of LiTFSI, *Angew. Chem.*, 2022, **134**, e202209169.

44 H. Sun, X. Xie, Q. Huang, Z. Wang, K. Chen, X. Li, J. Gao, Y. Li, H. Li, J. Qiu and W. Zhou, Fluorinated poly-oxalate electrolytes stabilizing both anode and cathode interfaces for all-solid-state Li/NMC811 batteries, *Angew. Chem., Int. Ed.*, 2021, **60**, 18335–18343.

45 W. Gu, G. Xue, Q. Dong, R. Yi, Y. Mao, L. Zheng, H. Zhang, X. Fan, Y. Shen and L. Chen, Trimethoxyboroxine as an electrolyte additive to enhance the 4.5 V cycling performance of a Ni-rich layered oxide cathode, *eScience*, 2022, **2**, 486–493.

46 Y. Jiang, C. Qin, P. Yan and M. Sui, Origins of capacity and voltage fading of $LiCoO_2$ upon high voltage cycling, *J. Mater. Chem. A*, 2019, **7**, 20824–20831.

47 L. Li, D. Wang, G. Xu, Q. Zhou, J. Ma, J. Zhang, A. Du, Z. Cui, X. Zhou and G. Cui, Recent progress on electrolyte functional additives for protection of nickel-rich layered oxide cathode materials, *J. Energy Chem.*, 2022, **65**, 280–292.

48 H. Luo, B. Zhang, H. Zhang, Q. Zheng, X. Wu, Y. Yan, Z. Li, Y. Tang, W. Hao, G. Liu, Y.-h. Hong, J. Ye, Y. Qiao and S.-G. Sun, Full-dimensional analysis of electrolyte decomposition on cathode–electrolyte interface: Establishing characterization paradigm on $LiNi_{0.6}Co_{0.2}Mn_{0.2}O_2$ cathode with potential dependence, *J. Phys. Chem. Lett.*, 2023, **14**, 4565–4574.

49 M. Mao, B. Huang, Q. Li, C. Wang, Y.-B. He and F. Kang, In-situ construction of hierarchical cathode electrolyte interphase for high performance $LiNi_{0.8}Co_{0.1}Mn_{0.1}O_2$/Li metal battery, *Nano Energy*, 2020, **78**, 105282.

50 G. Chen, L. Qiao, G. Xu, L. Li, J. Li, L. Li, X. Liu, Z. Cui, S. Zhang, S. Cheng, C. Han, S. Wang, X. Zhou and G. Cui, A highly-fluorinated lithium borate main salt empowering stable lithium metal batteries, *Angew. Chem., Int. Ed.*, 2024, **63**, e202400797.

51 Z. Li, H. Rao, R. Atwi, B. M. Sivakumar, B. Gwalani, S. Gray, K. S. Han, T. A. Everett, T. A. Ajantiwalay, V. Murugesan, N. N. Rajput and V. G. Pol, Non-polar ether-based electrolyte solutions for stable high-voltage non-aqueous lithium metal batteries, *Nat. Commun.*, 2023, **14**, 868.

52 J. Xu, Critical review on cathode-electrolyte interphase toward high-voltage cathodes for Li-ion batteries, *Nano-Micro Lett.*, 2022, **14**, 166.

53 J. Huang, J. Liu, J. He, M. Wu, S. Qi, H. Wang, F. Li and J. Ma, Optimizing electrode/electrolyte interphases and Li-ion flux/solvation for lithium-metal batteries with qua-functional heptafluorobutyric anhydride, *Angew. Chem., Int. Ed.*, 2021, **60**, 20717–20722.

54 C. Niu, H. Lee, S. Chen, Q. Li, J. Du, W. Xu, J.-G. Zhang, M. S. Whittingham, J. Xiao and J. Liu, High-energy lithium metal pouch cells with limited anode swelling and long stable cycles, *Nat. Energy*, 2019, **4**, 551–559.

55 Z. Jiang, Z. Zeng, X. Liang, L. Yang, W. Hu, C. Zhang, Z. Han, J. Feng and J. Xie, Fluorobenzene, a low-density, economical, and bifunctional hydrocarbon cosolvent for

practical lithium metal batteries, *Adv. Funct. Mater.*, 2021, **31**, 2005991.
56 D.-J. Yoo, S. Yang, K. J. Kim and J. W. Choi, Fluorinated aromatic diluent for high-performance lithium metal batteries, *Angew. Chem., Int. Ed.*, 2020, **59**, 14869–14876.
57 H. Zhang, Z. Zeng, R. He, Y. Wu, W. Hu, S. Lei, M. Liu, S. Cheng and J. Xie, 1,3,5-Trifluorobenzene and fluorobenzene co-assisted electrolyte with thermodynamic and interfacial stabilities for high-voltage lithium metal battery, *Energy Storage Mater.*, 2022, **48**, 393–402.
58 F. Meng, H. Zhang, X. Xiong, X. Li, R. Wu, Q. Han, B. Qin, B. Yuan and R. Hu, Revealing the subzero-temperature electrochemical kinetics behaviors in Ni-rich cathode, *Small*, 2024, **20**, 2304806.
59 Z. Cui, Z. Guo and A. Manthiram, Irreparable interphase chemistry degradation induced by temperature pulse in lithium-ion batteries, *Angew. Chem., Int. Ed.*, 2023, **62**, e202313437.
60 N. Phattharasupakun, P. Bunyanidhi, P. Chiochan, N. Chanlek and M. Sawangphruk, Effect of charging protocols on electrochemical performance and failure mechanism of commercial level Ni-rich NMC811 thick electrode, *Electrochem. Commun.*, 2022, **139**, 107309.
61 M. Golozar, A. Paolella, H. Demers, S. Bessette, M. Lagacé, P. Bouchard, A. Guerfi, R. Gauvin and K. Zaghib, In-situ observation of solid electrolyte interphase evolution in a lithium metal battery, *Commun. Chem.*, 2019, **2**, 1–9.
62 C. Gong, S. D. Pu, X. Gao, S. Yang, J. Liu, Z. Ning, G. J. Rees, I. Capone, L. Pi, B. Liu, G. O. Hartley, J. Fawdon, J. Luo, M. Pasta, C. R. M. Grovenor, P. G. Bruce and A. W. Robertson, Revealing the role of fluoride-rich battery electrode interphases by operando transmission electron microscopy, *Adv. Energy Mater.*, 2021, **11**, 2003118.
63 X. Zhang, Z. Guo, X. Li, Q. Liu, H. Hu, F. Li, Q. Huang, L. Zhang, Y. Tang and J. Huang, Cryo-ultramicrotomy enables TEM characterization of global lithium/polymer interfaces, *Energy Environ. Sci.*, 2024, **17**, 1436–1447.
64 J. Han, M. J. Lee, J. H. Min, K. H. Kim, K. Lee, S. H. Kwon, J. Park, K. Ryu, H. Seong, H. Kang, E. Lee, S. W. Lee and B. J. Kim, Fluorine-containing phase-separated polymer electrolytes enabling high-energy solid-state lithium metal batteries, *Adv. Funct. Mater.*, 2024, **34**, 2310801.
65 H. Peng, T. Long, J. Peng, H. Chen, L. Ji, H. Sun, L. Huang and S. G. Sun, Molecular design for in-situ polymerized solid polymer electrolytes enabling stable cycling of lithium metal batteries, *Adv. Energy Mater.*, 2024, **14**, 2400428.
66 J. Hu, L. Li, E. Hu, S. Chae, H. Jia, T. Liu, B. Wu, Y. Bi, K. Amine, C. Wang, J. Zhang, J. Tao and J. Xiao, Mesoscale-architecture-based crack evolution dictating cycling stability of advanced lithium ion batteries, *Nano Energy*, 2021, **79**, 105420.
67 F. Wang, Tracking lithium transport and electrochemical reactions in nanoparticles, *Nat. Commun.*, 2012, **3**, 1201.
68 Z. He, W. Li, Y. Chen, F. Huang, Y. Jie, X. Li, R. Cao and S. Jiao, Nanoscale characterization of the solid electrolyte interphase and lithium growth by atomic force microscopy, *Battery Energy*, 2024, **3**, 20230045.
69 M. Wang, Z. Song, J. Bi, H. Li, M. Xu, Y. Gong, Y. Zhou, Y. Zhao and K. Yang, Probing interfacial electrochemistry by in-situ atomic force microscope for battery characterization, *Battery Energy*, 2023, **2**, 20230006.
70 X. Shen, R. Zhang, X. Chen, X. B. Cheng, X. Li and Q. Zhang, The failure of solid electrolyte interphase on Li metal anode: Structural uniformity or mechanical strength?, *Adv. Energy Mater.*, 2020, **10**, 1903645.
71 S. Yuan, S. Weng, F. Wang, X. Dong, Y. Wang, Z. Wang, C. Shen, J. L. Bao, X. Wang and Y. Xia, Revisiting the designing criteria of advanced solid electrolyte interphase on lithium metal anode under practical condition, *Nano Energy*, 2021, **83**, 105847.
72 Q.-K. Zhang, X.-Q. Zhang, J. Wan, N. Yao, T.-L. Song, J. Xie, L.-P. Hou, M.-Y. Zhou, X. Chen, B.-Q. Li, R. Wen, H.-J. Peng, Q. Zhang and J.-Q. Huang, Homogeneous and mechanically stable solid–electrolyte interphase enabled by trioxane-modulated electrolytes for lithium metal batteries, *Nat. Energy*, 2023, **8**, 725–735.
73 J.-X. Tian, H.-J. Guo, J. Wan, G.-X. Liu, R. Wen and L.-J. Wan, In-situ analysis of dynamic evolution of the additive-regulated cathode processes in quasi-solid-state lithium-metal batteries, *Sci. China: Chem.*, 2023, **66**, 2921–2928.
74 W. Lu, J. Zhang, J. Xu, X. Wu and L. Chen, In-situ visualized cathode electrolyte interphase on $LiCoO_2$ in high voltage cycling, *ACS Appl. Mater. Interfaces*, 2017, **9**, 19313–19318.
75 M. Chen, W. Wang, Z. Shi, Z. Liu and C. Shen, Revealing the cathode electrolyte interphase on Li- and Mn-rich materials by in-situ electrochemical atomic force microscopy, *Appl. Surf. Sci.*, 2022, **600**, 154119.
76 J. Zhang, S. Li, X. Wang, S. Mao, J. Guo, Z. Shen, J. Mao, Q. Wu, K. Shen, H. Cheng, Y. Tan and Y. Lu, Construction of stable Li_2O-rich solid electrolyte interphase for practical PEO-based Li-metal batteries, *Adv. Energy Mater.*, 2024, **14**, 2302587.
77 Q. Wu, M. Fang, S. Jiao, S. Li, S. Zhang, Z. Shen, S. Mao, J. Mao, J. Zhang, Y. Tan, K. Shen, J. Lv, W. Hu, Y. He and Y. Lu, Phase regulation enabling dense polymer-based composite electrolytes for solid-state lithium metal batteries, *Nat. Commun.*, 2023, **14**, 6296.
78 W. Chen, X. Xiong, R. Zeng, L. Jiang, Z. Chen, Z. Xiao, L. Qie, F. Yu and Y. Huang, Enhancing the interfacial ionic transport via in-situ 3D composite polymer electrolytes for solid-state lithium batteries, *ACS Appl. Energy Mater.*, 2020, **3**, 7200–7207.
79 S. Qin, Y. Yu, J. Zhang, Y. Ren, C. Sun, S. Zhang, L. Zhang, W. Hu, H. Yang and D. Yang, Separator-free In-situ dual-curing solid polymer electrolytes with enhanced interfacial contact for achieving ultrastable lithium-metal batteries, *Adv. Energy Mater.*, 2023, **13**, 2301470.
80 F. Ding, W. Xu, G. L. Graff, J. Zhang, M. L. Sushko, X. Chen, Y. Shao, M. H. Engelhard, Z. Nie, J. Xiao, X. Liu, P. V. Sushko, J. Liu and J.-G. Zhang, Dendrite-free lithium deposition via self-healing electrostatic shield mechanism, *J. Am. Chem. Soc.*, 2013, **135**, 4450–4456.

81 W. Xu, W. Dong, J. Lin, K. Mu, Z. Song, J. Tan, R. Wang, Q. Liu, C. Zhu, J. Xu and L. Tian, Optimization design of fluoro-cyanogen copolymer electrolyte to achieve 4.7 V high-voltage solid lithium metal battery, *Adv. Sci.*, 2024, 2400466, DOI: **10.1002/advs.202400466**.

82 S. Qin, Z. Wang, Y. Ren, Y. Yu, Y. Xiao, J. Chen, J. Zhang, S. Zhang, C. Sun, J. Xiao, L. Zhang, W. Hu and H. Yang, A meltblown cloth reinforced partially fluorinated solid polymer electrolyte for ultrastable lithium metal batteries, *Nano Energy*, 2024, **119**, 109075.

83 K. Yang, Z. Shen, J. Huang, J. Zhong, Y. Lin, J. Zhu, J. Chen, Y. Wang, T. Xie, J. Li and Z. Shi, In-situ fabrication of fluorine-modified acrylate-based gel polymer electrolytes for lithium-metal batteries, *Mater. Chem. Front.*, 2023, **7**, 4152–4163.

84 C. Monroe and J. Newman, The impact of elastic deformation on deposition kinetics at lithium/polymer interfaces, *J. Electrochem. Soc.*, 2005, **152**, A396.

85 C. Fang, B. Lu, G. Pawar, M. Zhang, D. Cheng, S. Chen, M. Ceja, J.-M. Doux, H. Musrock, M. Cai, B. Liaw and Y. S. Meng, Pressure-tailored lithium deposition and dissolution in lithium metal batteries, *Nat. Energy*, 2021, **6**, 987–994.

86 G. Li and N. S. Sampson, Alternating ring-opening metathesis polymerization (AROMP) of hydrophobic and hydrophilic monomers provides oligomers with side-chain sequence control, *Macromolecules*, 2018, **51**, 3932–3940.

87 Z. Zhang, L. Xia, T.-Y. Zeng, D.-C. Wu, W.-J. Zhang, C.-Y. Hong and Y.-Z. You, Hybrid copolymerization via mechanism interconversion between radical vinyl-addition and anion ring-opening polymerization, *Polym. Chem.*, 2019, **10**, 2117–2125.

88 S. Wang, L. Zhang, Q. Zeng, J. Guan, H. Gao, L. Zhang, J. Zhong, W. Y. Lai and Q. Wang, Designing polymer electrolytes via ring-opening polymerization for advanced lithium batteries, *Adv. Energy Mater.*, 2024, **14**, 2302876.

89 P. J. Flory, Molecular size distribution in ethylene oxide polymers, *J. Am. Chem. Soc.*, 1940, **62**, 1561–1565.

90 C. Billouard, S. Carlotti, P. Desbois and A. Deffieux, Controlled high-speed anionic polymerization of propylene oxide initiated by alkali metal alkoxide/trialkylaluminum systems, *Macromolecules*, 2004, **37**, 4038–4043.

91 M. Singh, O. Odusanya, G. M. Wilmes, H. B. Eitouni, E. D. Gomez, A. J. Patel, V. L. Chen, M. J. Park, P. Fragouli, H. Iatrou, N. Hadjichristidis, D. Cookson and N. P. Balsara, Effect of molecular weight on the mechanical and electrical properties of block copolymer electrolytes, *Macromolecules*, 2007, **40**, 4578–4585.

92 A. A. Teran, M. H. Tang, S. A. Mullin and N. P. Balsara, Effect of molecular weight on conductivity of polymer electrolytes, *Solid State Ionics*, 2011, **203**, 18–21.

93 P. Dreier, A. Pipertzis, M. Spyridakou, R. Mathes, G. Floudas and H. Frey, Introduction of trifluoromethanesulfonamide groups in poly(ethylene oxide): Ionic conductivity of single-ion-conducting block copolymer electrolytes, *Macromolecules*, 2022, **55**, 1342–1353.

94 A. Krimalowski and M. Thelakkat, Sequential Co-click reactions with poly(glycidyl propargyl ether) toward single-ion conducting electrolytes, *Macromolecules*, 2019, **52**, 4042–4051.

95 C. Wölke, D. Diddens, B. Heidrich, M. Winter and I. Cekic-Laskovic, Understanding the effectiveness of phospholane electrolyte additives in lithium-ion batteries under high-voltage conditions, *ChemElectroChem*, 2021, **8**, 972–982.

96 C.-C. Su, M. He, C. Peebles, L. Zeng, A. Tornheim, C. Liao, L. Zhang, J. Wang, Y. Wang and Z. Zhang, Functionality selection principle for high voltage lithium-ion battery electrolyte additives, *ACS Appl. Mater. Interfaces*, 2017, **9**, 30686–30695.

97 Q. Zheng, Y. Yamada, R. Shang, S. Ko, Y.-Y. Lee, K. Kim, E. Nakamura and A. Yamada, A cyclic phosphate-based battery electrolyte for high voltage and safe operation, *Nat. Energy*, 2020, **5**, 291–298.

98 N. Von Aspern, D. Diddens, T. Kobayashi, M. Börner, O. Stubbmann-Kazakova, V. Kozel, G.-V. Röschenthaler, J. Smiatek, M. Winter and I. Cekic-Laskovic, Fluorinated cyclic phosphorus(iii)-based electrolyte additives for high voltage application in lithium-ion batteries: Impact of structure–reactivity relationships on CEI formation and cell performance, *ACS Appl. Mater. Interfaces*, 2019, **11**, 16605–16618.

99 P. Olsén, K. Odelius and A.-C. Albertsson, Thermodynamic presynthetic considerations for ring-opening polymerization, *Biomacromolecules*, 2016, **17**, 699–709.

100 H. Yang, B. Zhang, M. Jing, X. Shen, L. Wang, H. Xu, X. Yan and X. He, In-situ catalytic polymerization of a highly homogeneous PDOL composite electrolyte for long-cycle high-voltage solid-state lithium batteries, *Adv. Energy Mater.*, 2022, **12**, 2201762.

101 E. Zinigrad, L. Larush-Asraf, J. S. Gnanaraj, M. Sprecher and D. Aurbach, On the thermal stability of $LiPF_6$, *Thermochim. Acta*, 2005, **438**, 184–191.

102 W. Li, J. Gao, H. Tian, X. Li, S. He, J. Li, W. Wang, L. Li, H. Li, J. Qiu and W. Zhou, SnF_2-catalyzed formation of polymerized dioxolane as solid electrolyte and its thermal decomposition behavior, *Angew. Chem., Int. Ed.*, 2022, **61**, e202114805.

103 J. Zhu, R. Zhao, J. Zhang, X. Song, J. Liu, N. Xu, H. Zhang, X. Wan, X. Ji, Y. Ma, C. Li and Y. Chen, Long-cycling and high-voltage solid state lithium metal batteries enabled by fluorinated and crosslinked polyether electrolytes, *Angew. Chem., Int. Ed.*, 2024, **63**, e202400303.

104 Z. Chen, J. Xian, X. Pan, F. Ren, Y. Li, Y. Tan, Y. Bai and J. Wu, Lithium metal batteries with in-situ copolymerized fluorinated polyether electrolytes, *J. Mater. Chem. A*, 2023, **11**, 26794–26803.

105 P. Li, S. Wang, J. Hao, X. Wang, S.-M. Hao, Y. Lu, H. Li, W. Zhou and Y. Li, Efficiencies of various in-situ polymerizations of liquid electrolytes and the practical implications for quasi solid-state batteries, *Angew. Chem., Int. Ed.*, 2023, **62**, e202309613.

106 Q. Zhao, X. Liu, S. Stalin, K. Khan and L. A. Archer, Solid-state polymer electrolytes with in-built fast interfacial transport for secondary lithium batteries, *Nat. Energy*, 2019, **4**, 365–373.

107 S. Jiao, X. Ren, R. Cao, M. H. Engelhard, Y. Liu, D. Hu, D. Mei, J. Zheng, W. Zhao, Q. Li, N. Liu, B. D. Adams, C. Ma, J. Liu, J.-G. Zhang and W. Xu, Stable cycling of high-voltage lithium metal batteries in ether electrolytes, *Nat. Energy*, 2018, **3**, 739–746.

108 H. Wang, Z. Yu, X. Kong, W. Huang, Z. Zhang, D. G. Mackanic, X. Huang, J. Qin, Z. Bao and Y. Cui, Dual-solvent Li-ion solvation enables high-performance Li-metal batteries, *Adv. Mater.*, 2021, **33**, 2008619.

109 J. Yan, P. F. Marina and A. Blencowe, Influence of polymerisation conditions on the kinetics of poly(lactic-co-glycolic acid)-b-poly(ethylene glycol)-b-poly(lactic-co-glycolic acid) triblock synthesis and the occurrence of transesterification side reactions, *Polym. Chem.*, 2023, **14**, 2229–2237.

110 S. Chatani, C. J. Kloxin and C. N. Bowman, The power of light in polymer science: Photochemical processes to manipulate polymer formation, structure, and properties, *Polym. Chem.*, 2014, **5**, 2187–2201.

111 T. B. Stachowiak, F. Svec and J. M. J. Fréchet, Patternable protein resistant surfaces for multifunctional microfluidic devices via surface hydrophilization of porous polymer monoliths using photografting, *Chem. Mater.*, 2006, **18**, 5950–5957.

112 Y. Xie, K. Zhang, Y. Yamauchi, K. Oyaizu and Z. Jia, Nitroxide radical polymers for emerging plastic energy storage and organic electronics: Fundamentals, materials, and applications, *Mater. Horiz.*, 2021, **8**, 803–829.

113 X. Zheng, S. Ma, Y. Zhang, W. Lin, K. Ji, C. Wang and M. Chen, In-situ polymerization of fluorinated polyacrylate copolymer solid electrolytes for high-voltage lithium metal batteries at room temperature, *Macromolecules*, 2023, **56**, 1077–1085.

114 K. Guo, S. Li, J. Wang, Z. Shi, Y. Wang and Z. Xue, In-situ orthogonal polymerization for constructing fast-charging and long-lifespan Li metal batteries with topological copolymer electrolytes, *ACS Energy Lett.*, 2024, **9**, 843–852.

115 J. Park, H. Seong, C. Yuk, D. Lee, Y. Byun, E. Lee, W. Lee and B. J. Kim, Design of fluorinated elastomeric electrolyte for solid-state lithium metal batteries operating at low temperature and high voltage, *Adv. Mater.*, 2024, 2403191, DOI: **10.1002/adma.202403191**.

116 A. Hu, W. Chen, F. Li, M. He, D. Chen, Y. Li, J. Zhu, Y. Yan, J. Long, Y. Hu, T. Lei, B. Li, X. Wang and J. Xiong, Nonflammable polyfluorides-anchored quasi-solid electrolytes for ultra-safe anode-free lithium pouch cells without thermal runaway, *Adv. Mater.*, 2023, **35**, 2304762.

117 B. Yang, Y. Pan, T. Li, A. Hu, K. Li, B. Li, L. Yang and J. Long, High-safety lithium metal pouch cells for extreme abuse conditions by implementing flame-retardant perfluorinated gel polymer electrolytes, *Energy Storage Mater.*, 2024, **65**, 103124.

118 S. Zhang, S. Li and Y. Lu, Designing safer lithium-based batteries with nonflammable electrolytes: A review, *eScience*, 2021, **1**, 163–177.

119 Y. Lin, Z. Shen, J. Huang, J. Zhu, S. Jiang, S. Zhan, Y. Xie, J. Chen and Z. Shi, In-situ construction of fluorine-containing modified gel polymer electrolyte with high interfacial stability for high-rate lithium metal battery, *J. Power Sources*, 2023, **584**, 233612.

120 J. Huang, Z. Shen, S. J. Robertson, Y. Lin, J. Zhu, K. Yang, Y. Wang, M. Shao and Z. Shi, Fluorine grafted gel polymer electrolyte by in-situ construction for high-voltage lithium metal batteries, *Chem. Eng. J.*, 2023, **475**, 145802.

121 N. Xu, Y. Zhao, M. Ni, J. Zhu, X. Song, X. Bi, J. Zhang, H. Zhang, Y. Ma, C. Li and Y. Chen, In-situ cross-linked F-and P-containing solid polymer electrolyte for long-cycling and high-safety lithium metal batteries with various cathode materials, *Angew. Chem., Int. Ed.*, 2024, **63**, e202404400.

122 F.-N. Jiang, X.-B. Cheng, S.-J. Yang, J. Xie, H. Yuan, L. Liu, J.-Q. Huang and Q. Zhang, Thermoresponsive electrolytes for safe lithium-metal batteries, *Adv. Mater.*, 2023, **35**, 2209114.

123 J. Merna, P. Vlček, V. Volkis and J. Michl, Li+ catalysis and other new methodologies for the radical polymerization of less activated olefins, *Chem. Rev.*, 2016, **116**, 771–785.

124 H. Xu, J. Yang, Y. Niu, X. Hou, Z. Sun, C. Jiang, Y. Xiao, C. He, S. Yang, B. Li and W. Chen, Deciphering and integrating functionalized side chains for high ion-conductive elastic ternary copolymer solid-state electrolytes for safe lithium metal batteries, *Angew. Chem., Int. Ed.*, 2024, e202406637, DOI: **10.1002/anie.202406637**.

125 Y. Wang, S. Chen, Z. Li, C. Peng, Y. Li and W. Feng, In-situ generation of fluorinated polycarbonate copolymer solid electrolytes for high-voltage Li-metal batteries, *Energy Storage Mater.*, 2022, **45**, 474–483.

126 R. Lin, Y. He, C. Wang, P. Zou, E. Hu, X.-Q. Yang, K. Xu and H. L. Xin, Characterization of the structure and chemistry of the solid–electrolyte interface by cryo-EM leads to high-performance solid-state Li-metal batteries, *Nat. Nanotechnol.*, 2022, **17**, 768–776.